https://doi.org/10.5194/acp-2021-646
Preprint. Discussion started: 25 August 2021

Atmospheric Chemistry and Physics Discussions

Analyzing ozone variations and uncertainties at high latitudes during Sudden Stratospheric Warming events using MERRA-2

Shima Bahramvash Shams[1,2], Von P. Walden[1], James W Hannigan[2], William J. Randel[2], Irina V. Petropavlovskikh[3,4], Amy H. Butler[5], Alvaro de la Cámara[6]

[1] Washington State University, Pullman, WA, United States,
[2] NCAR, National Center for Atmospheric Research, Boulder, CO, United States,
[3] Cooperative Institute for Research in Environmental Sciences, University of Colorado, Boulder, CO, USA
[4] National Oceanic and Atmospheric Administration, Global Monitoring Division, Boulder, CO, USA
[5] National Oceanic and Atmospheric Administration, Chemical Sciences Laboratory, Boulder, CO, USA
[6] Dept. Física de la Tierra y Astrofísica, Universidad Complutense de Madrid, Madrid, Spain

Corresponding author: Shima Bahramvash Shams, s.bahramvashshams@wsu.edu

Abstract:

Stratospheric circulation is a critical part of the Arctic ozone cycle. Sudden stratospheric warming events (SSWs) manifest the strongest alteration of stratospheric dynamics. Changes in planetary wave propagation vigorously influence zonal mean zonal wind, temperature, and tracer concentrations in the stratosphere over the high latitudes. In this study, we examine six major SSWs from 2004 to 2020 using the Modern-Era Retrospective analysis for Research and Applications, Version 2 (MERRA-2). Using the unique density of observations around the Greenland sector at high latitudes, we perform comprehensive comparisons of high latitude observations with the MERRA-2 ozone dataset during the six major SSWs. Our results show that MERRA-2 captures the high variability of mid stratospheric ozone fluctuations during SSWs over high latitudes. However, larger uncertainties are observed in the lower stratosphere and troposphere. The zonally averaged stratospheric ozone shows a dramatic increase of 9-29% in total column ozone (TCO) near the time of each SSW, which lasts up to two months. The SSWs exhibit a more significant impact on ozone over high northern latitudes when the polar vortex is mostly elongated as seen in 2009 and 2018 compared to the events in which the polar vortex is displaced

https://doi.org/10.5194/acp-2021-646
Preprint. Discussion started: 25 August 2021


Atmospheric Chemistry and Physics Discussions

towards Europe. The regional impact of SSWs over Greenland has a similar structure as the zonal average, however, exhibits more intense ozone anomalies which is reflected by 15-37% increase in TCO. The influence of SSW on mid stratospheric ozone levels persists longer than their impact on temperature. This paper is focused on the increased (suppressed) wave activity before (after) the SSWs and their impact on ozone variability at high latitudes. This includes an investigation of the different terms of tracer continuity using MERRA-2 parameters, which emphasizes the key role of vertical advection on mid-stratospheric ozone during the SSWs.

1. Introduction

Stratospheric ozone can modulate the radiative forcing of climate and Earth's surface temperature (Haigh, 1994; Ramaswamy et al., 1996; Smith and Polvani, 2014; Calvo et al., 2015; Kidston et al., 2015; Nowack et al., 2015; Romanowsky et al., 2019). High latitude stratospheric ozone influences tropospheric climate, surface temperature of lower latitudes, El Niño-Southern Oscillation (ENSO) events, and the North Pacific Oscillation (NPO) (Baldwin and Dunkerton, 2001; Ineson and Scaife, 2008; Cagnazzo and Manzini, 2009; Karpechko et al., 2014; Xie et al., 2016). Thus, it is important to have a thorough understanding of high latitude ozone variations.

Dynamical variability plays a critical role in fluctuations of stratospheric ozone (Holton et al., 1995; Fusco and Salby, 1999; Rao et al., 2004; Bahramvash-Shams et al., 2019). Planetary waves modulate poleward ozone transport through the Brewer-Dobson circulation (BDC) (Lindzen and Holton, 1968; Holton and Lindzen, 1972; Wallace, 1973; Holton et al., 1995). The BDC transports tropical stratospheric air parcels with high ozone concentrations to the high-latitude stratosphere, causing ozone accumulation during winter and peak values in the spring (Rao, 2003; Rao et al., 2004). Sudden stratospheric warming events (SSWs) are the largest alterations of stratospheric circulation during wintertime and a significant factor in the interannual variability of stratospheric transport (Schoeberl, 1978; Butler et al., 2015; de la Cámara et al., 2018a).

https://doi.org/10.5194/acp-2021-646
Preprint. Discussion started: 25 August 2021


Atmospheric Chemistry and Physics Discussions

SSWs are defined as an abrupt and intense stratospheric temperature increase that coincides with a reversal of the climatological westerly wind circulation (Scherhag, 1952, Baldwin et al. 2021). Although the current understanding of the mechanisms that induce SSWs is still uncertain (de la Cámara et al., 2019; Lawrence and Manney, 2020), increased vertical propagation of planetary-scale waves from the extratropical troposphere into the stratosphere over high latitudes is closely related to these abrupt events (Matsuno, 1971; Schoeberl, 1978; Scott and Polvani, 2004). However, the occurrence of SSWs is shown to be sensitive to many other factors such as lower stratosphere conditions, the geometry of the polar vortex, the gradient of potential vorticity (PV) at the edge of the polar vortex, and synoptic systems at lower altitudes (Tripathi et al. 2015, de la Cámara et al., 2019; Lawrence and Manney, 2020). Changes in momentum deposition associated with these processes leads to the rapid deceleration and disruption of the stratospheric polar vortex, typically by either splitting the vortex into two smaller lobes or displacing the vortex off the pole (Matsuno, 1971; Polvani and Waugh, 2004; Charlton and Polvani, 2007). The altered circulation during SSWs impacts the transportation of trace gases (Randel 1993, de la Cámara et al., 2018b), can influence tropospheric weather and climate (Baldwin and Dunkerton, 2001; Butler et al., 2017; Charlton-Perez et al., 2018, Butler and Domeisen 2021), and gravity waves over the Arctic (Thurairajah et al., 2010) and consequently the pole-to-pole circulation (Houghton, 1978; Fritts and Alexander, 2003). SSWs are one of the strongest manifestations of atmospheric coupling. These large-scale altered circulations perturb the mesosphere by cooling it and consequently lowering the stratopause by up to 30 km (Manney et al., 2008b). Dynamical coupling between the stratosphere and troposphere is another important consequence of SSWs with implications for surface climate predictability on subseasonal timescales (Baldwin and Dunkerton 2001, Butler et al. 2019).

The Modern Era Retrospective Analysis for Research and Application, version 2 (MERRA-2) is used to investigate ozone fluctuations during SSWs. Previous validation of MERRA-2 ozone data with ozonesondes and satellite data over the South Pole and midlatitudes has shown good correlation (Gelaro et al., 2017; Wargan et al., 2017). However, MERRA-2 ozone data are expected to have higher uncertainties over the northern high latitudes because of higher

https://doi.org/10.5194/acp-2021-646
Preprint. Discussion started: 25 August 2021


Atmospheric Chemistry and Physics Discussions

dynamic variability in this region (Wargan et al., 2017). During SSWs, the alteration of dynamical processes causes dramatic variability in trace gas concentrations in the middle atmosphere. The complexity of altered dynamics of SSWs might introduce extra uncertainties into the numerical and assimilation models. The performance of MERRA-2 ozone products during SSWs has not been investigated in previous studies. It is essential to understand the performance of MERRA-2 ozone simulations during these anomalous events before using them for further analysis of ozone variations.

Various studies have focused on individual SSWs, their evolution, and dynamical characteristics (Siskind et al., 2007; Manney et al., 2008a; Coy et al., 2009; Manney et al., 2009b). Some studies have investigated ozone transport during SSWs based on modeling and simulation (Tao et al, 2015; de la Cámara et al., 2018 a and b; Oehrlein et al, 2020). A few studies used observations to investigate local (Flury et al., 2009; Scheiben et al 2012; Schranz et al 2020) or zonal impacts of specific SSW events on ozone (Manney et al 2009a; Manney et al, 2015). Numerical models have shown the influence of SSWs on stratospheric transport and mixing over high latitudes (Tao et al., 2015; de la Cámara et al., 2018b). This study investigates zonal average ozone variations (between 60 and 80 N) during six SSWs using the MERRA-2 dataset.

This study focuses on using observations and an assimilation model to analyze and compare the impact of SSWs on ozone from 2004 to 2020. During SSWs, MERRA-2 ozone data are compared with in situ and ground-based remote sensing observations from high northern latitudes. The advantage of an existing dense network of observations around the Greenland sector at high latitudes (Figure 1) provides an opportunity to explore the uncertainties of MERRA-2 ozone profiles over high latitudes during SSWs. These comparisons provide a thorough understanding of the uncertainties in the MERRA-2 dataset in this region and, in particular, during extreme dynamic events.

In section 2, MERRA-2 and other independent observations are described. The methodology of comparisons and dynamical analysis are presented in section 3. The results of the comparison between MERRA-2 and independent observation are discussed in section 4. The

https://doi.org/10.5194/acp-2021-646
Preprint. Discussion started: 25 August 2021


Atmospheric Chemistry and Physics Discussions

evolution of each SSW and its impact on ozone are discussed in section 5. Discussion of transport mechanisms is provided in section 6. Section 7 presents the conclusions of this research study.

2. Data

The Modern-Era Retrospective Analysis for Research and Application, version 2 (MERRA-2) from NASA's Global Monitoring and Assimilation Office (GMAO) uses the Goddard Earth Observing System, Version 5 (GEOS5) atmospheric data assimilation system (Molod et al., 2015; Gelaro et al., 2017). A variety of data sets and models are incorporated in MERRA-2 to create 3-dimensional ozone datasets with a time-frequency of 3 hours, including ozone and meteorological observations, global circulation models, and extended reanalysis (Wargan et al., 2017; Gelaro et al., 2017). Total column ozone from the Solar Backscatter Ultraviolet Radiometer (SBUV) (1980 to 2004) and the Ozone Monitoring Instrument (OMI) (since 2004) and retrieved ozone profiles from SBUV (1980 to 2004) and the Microwave Limb Sounder (MLS) (since 2004) are used to estimate ozone in MERRA-2 (Gelaro et al., 2017). MERRA-2 data are available online through the NASA Goddard Earth Sciences Data Information Services Center (GES DISC; http://disc.sci.gsfc.nasa.gov/ daac-bin/DataHoldings.pl).

MERRA-2 has been used extensively to study ozone trends and processes (Coy et al., 2016; Knowland et al., 2017; Wargan et al., 2018; Shangguan et al., 2019). In this study, the ozone dataset from the MERRA-2 reanalyses at a spatial resolution of $0.5^{\circ} \times 0.625^{\circ}$ will be used. To investigate dynamical mechanisms, temperature, the northward wind (v), vertical pressure velocity (ω), potential temperature (θ, calculated from temperature and pressure), and potential vorticity (PV) are extracted from the pressure-level MERRA-2 dataset.

In assimilated/reanalysis models such as MERRA-2, variations in models, methods of analysis, and observations cause uncertainties in the products (Rienecker et al., 2011). Previously MERRA-2 ozone data was validated using ozonesondes and satellite data from 2005 to 2012 (Gelaro et al., 2017; Wargan et al., 2017). MERRA-2 agreement with independent observations has been improved since 2005 by assimilating OMI and MLS. Comparison with independent satellite observations show an average standard deviation of the differences of 5% and 11% in the

https://doi.org/10.5194/acp-2021-646
Preprint. Discussion started: 25 August 2021


Atmospheric Chemistry and Physics Discussions

upper and lower stratosphere, respectively (Wargan et al., 2017). The average standard deviation of 20% has been reported for the comparison between MERRA-2 lower stratospheric ozone and ozonesondes (Wargan et al., 2017). However, uncertainties are expected to be magnified at high latitudes because of higher dynamical variability (Wargan et al., 2017). Moreover, the anomalous atmospheric dynamics, displace/split polar vortex, and hemispherically asymmetric conditions during SSWs may cause unusual nonlinearity in ozone flux/transport terms. Thus, it is important to investigate the quality of MERRA-2 ozone simulations during highly altered circulations such as SSWs. This study provides a comprehensive comparison using ground-based remote sensing and in situ observations to MERRA-2 ozone datasets over northern high latitudes during SSWs. We also use a uniquely dense network of observations in the high latitudes to study a region of the Arctic that is climatologically important in terms of stratospheric circulation (Figure 1).

Ozonesondes have been used to monitor ozone for decades as the most direct measurement of the vertical ozone profile (Tiao et al., 1986; Logan, 1994; Logan et al., 1999; Stolarski, 2001; Gaudel et al., 2015; Bahramvash-Shams et al., 2019). Ozonesonde profiles provide a good standard for validation because they have high accuracy, fine vertical resolution of less than 100 m, year-round launches, and low sensitivity to clouds (McDonald et al., 1999; Ancellet et al., 2016; Sterling et al., 2017).

In this study, ozonesonde measurements at Eureka, Ny-Ålesund, Thule, and Summit will be used to investigate the uncertainties of MERRA-2. The locations of each station and the length of the ozonesonde measurements at each site are shown in Figure 1 and Table 1. Most of the ozonesonde measurements can be found at the World Ozone and Ultraviolet Radiation Data Centre (WOUDC), while ozonesonde data in the United States is obtained from NOAA's Earth System Research Laboratory including data from Summit Station, Greenland. The detailed description and uncertainty estimation of ozonesonde measurements have been discussed in previous studies (Komhyr, 1986; Johnson et al., 2002; Smit et al., 2007; Tarasick et al., 2016; Sterling et al., 2017).

In addition to ozonesondes, ground-based remote sensing data are also used in this paper to study the uncertainties in the MERRA-2 dataset. Retrieved ozone from ground-based Fourier

https://doi.org/10.5194/acp-2021-646
Preprint. Discussion started: 25 August 2021


Atmospheric Chemistry and Physics Discussions

transform infrared (FTIR) interferometers have been used for long term ozone analysis (Vigouroux et al., 2008; García et al., 2012; Vigouroux et al., 2015). In this study, ozone profiles retrieved from FTIR at five high-latitude sites (Eureka, Ny-Ålesund, Thule, Harestua, and Kiruna) were obtained from NDACC (Network for the Detection of Atmospheric Composition Change) and used to validate MERRA-2. The location of each site is shown in Figure 1 and Table 1. These datasets are available at http://www.ndacc.org.

The NDACC FTIR instruments measure solar radiation in a wide spectral bandwidth of 600-4500 cm^{-1} at a high spectral resolution of 0.0035 cm^{-1}. The retrieval of ozone profiles from NDACC FTIR instruments uses the optimal estimation method (Rodgers, 2000). NDACC retrievals use the spectroscopic database from HITRAN 2008 (Rothman et al., 2009). To retrieve trace gas information from the measured spectra using optimal estimation, additional information is required to constrain the result and find the optimal answer. Meteorological parameters from the National Centers for Environmental Prediction (NCEP) and monthly trace gas profiles from the Whole Atmosphere Community Climate Model WACCM4 (Marsh et al., 2013) are used as a priori conditions. More details of the NDACC ozone retrieval steps, configuration, and instrument specifications are discussed by Vigouroux et al (2008; 2015). Having the ability to resolve the fine structure of solar radiation spectra allows the retrieval of a variety of trace gases using the NDACC solar FTIR. However, these instruments require sunlight and clear-sky conditions, which restricts observations to the polar day at high latitudes.

The retrieved total ozone column and the stratospheric partial columns from FTIR are expected to have uncertainties of 2% and 6%, respectively (Vigouroux et al., 2015; Bognar et al., 2019). This study updates the uncertainties found by previous studies by adding additional years of data and by focusing on three high latitude sites that contain both ozonesondes and FTIR measurements. The FTIR ozone retrievals showed a high correlation (~ 90%) in comparison to ozonesonde profiles measured at Eureka, Ny-Ålesund, and Thule, with uncertainties shown in Table 1. Overall, the uncertainties are slightly higher than the averaged uncertainties reported by Vigouroux et al (2015). This is more pronounced at Eureka due to the high solar zenith angle, and the possibility that, at times, the FTIR views a slant path through the atmosphere that extends

https://doi.org/10.5194/acp-2021-646
Preprint. Discussion started: 25 August 2021


Atmospheric Chemistry and Physics Discussions

through the edge of the polar vortex. More details of the ozone retrievals at Eureka can be found in Bognar et al (2019). As shown in Table 1, the NDACC retrievals are biased high when compared to the ozonesondes. Also, the bias is higher at Eureka (7%) than at either Ny-Ålesund (1%) and Thule (3%). These biases and standard deviations (shown in Table 1) are less than the differences between MERRA-2 and the ozonesondes (20%) discussed above, indicating that the NDACC FTIR ozone retrievals can be used to increase the robustness of the uncertainty analysis of the MERRA-2 ozone dataset.

3. Methods

In this section, the details of the different methods used in this study are discussed, including the comparison methodology, detection of SSWs, and the derivation of dynamical parameters used to investigate ozone transport.

To have comparable points, NDACC and in situ site locations, shown in Figure 1 and Table 1, are extracted from the nearest $0.5^{\circ} \times 0.625^{\circ}$ grid MERRA-2 ozone dataset. The nearest instantaneous 3-hourly MERRA-2 ozone dataset is compared to the associated ozonesonde profile and the FTIR-retrieved ozone. The MERRA-2 ozone data are compared to ozonesondes at the model levels, up to the maximum measured altitude. However, the vertical resolution of the remote sensing retrieval is often not similar to the model grid points, to apply the retrieval sensitivity to the model level prior to the comparison, the averaging kernel is used through the smoothing method (Rodgers and Connor, 2003). Averaging kernels characterize the vertical resolution and sensitivity of FTIR instruments to the atmospheric ozone variability at various altitudes (Rodgers, 2000). Equation 1 shows how the averaging kernel is applied with the model data to account for the sensitivity of retrievals (Rodgers and Connor, 2003), producing a smoothed ozone profile.

$$x_s = x_a + A\,(x_h - x_a) \qquad (1)$$

where x_s is the final smoothed ozone profile, x_h is the model estimated profile, and x_a and A are the a priori and averaging kernel of the retrieval respectively. The smoothing method effectively linearizes the ozone from the model using the averaging kernel of the retrieval around the a priori

https://doi.org/10.5194/acp-2021-646
Preprint. Discussion started: 25 August 2021


Atmospheric Chemistry and Physics Discussions

information (Rodgers and Connor, 2003). MERRA-2 data are interpolated to the vertical grid of the retrievals before Equation 1 is applied.

The high spectral resolution of the solar FTIR measurements makes it possible to retrieve partial ozone columns in addition to the total column ozone. Based on the mean average kernels at all 5 stations, four partial column ozone (PCO) are determined in this study over the following altitude regions: ground-8 km, 8-15 km, 15-22 km, 22-34 km. The PCO amounts are also used to analyze uncertainties in the MERRA-2 ozone dataset. The comparison results are discussed in section 4.

There are a variety of definitions for detecting major SSWs (Charlton & Polvani, 2007; Butler et al., 2015; Palmeiro et al. 2015). This study uses wintertime reversals of the daily-mean, zonal-mean zonal winds at 60N and 10 hPa from the MERRA-2 dataset (Butler et al., 2017). The dates of major SSWs since 2004 are calculated using MERRA-2 data following the method described by Charlton & Polvani (2007) and are shown in Table 2. Table 2 also includes the duration, magnitude of the easterly zonal wind, and the duration of polar vortex recovery for each SSW; all information is derived from MERRA-2 data. It should be noted that the duration of the easterly wind shown in Table 2 is not necessarily consecutive.

The dynamical transport mechanisms are also investigated for each of the major SSWs. The zonal mean tracer concentration is a balance between transport processes and the chemical sources and sinks as shown in the continuity equation of the Transformed Eulerian Mean (TEM) (Andrews et al, 1987):

$$\bar{x}_t = -\bar{v}^* \bar{x}_y - \overline{w}^* \bar{x}_z + e^{Z/H} \Delta . M + P - L \quad (2)$$

where $\bar{x}_t$ is the tracer tendency (in this case, ozone mixing ratio), $(\bar{v}^*, \overline{w}^*)$ are horizontal and vertical components of the residual circulation, z = -H ln(p/p0) in log-pressure height using a scale height H of 7 km, M is eddy transport vector, and P and L are chemical production and loss. The overbars stand for the zonal average. Subscript symbols denote partial derivatives [with respect to time (t) and height (z)]. The first two terms on the right-hand side of equation (2)

https://doi.org/10.5194/acp-2021-646
Preprint. Discussion started: 25 August 2021


Atmospheric Chemistry and Physics Discussions

represent the contribution of advective transport on ozone changes. The vertical component of residual circulation is the dominant contributor of advection ($\overline{w}^*$) and can be estimated using TEM (Andrews et al, 1987):

$$\overline{w}^* = \overline{w} + \frac{1}{a\cos\phi(\varphi)}\partial_\varphi\left(\cos(\varphi)\frac{\overline{v'\Theta'}}{\overline{\Theta_z}}\right) \quad (3)$$

where v and w are the meridional and vertical winds, θ is potential temperature, a is the earth radius, φ is the latitude. The prime denotes the departure from the zonal mean. The third term on the right side of equation (2) shows the impact of eddy mixing on ozone transport. M can be decomposed into vertical and meridional components M_z and M_y respectively: (Andrews et al., 1987):

$$M_y = -e^{(-z/H)}\left(\overline{v'x'} - \frac{\overline{v'\Theta'}}{\overline{\Theta_z}}\bar{x}_z\right) \quad (2.4)$$

$$M_z = -e^{(-z/H)}\left(\overline{w'x'} + \frac{\overline{v'\Theta'}}{\overline{\Theta_z}}\bar{x}_y\right) \quad (2.5)$$

This study investigates the impact of the dynamics on polar ozone concentrations during individual SSWs using MERRA-2 data. Because the impact of the chemical components on the evolution of ozone during SSWs is a less important factor below 30 km (de la Cámara et al 2018b), the dynamical analysis in this study will focus on altitudes below 30 km. Thus, the lack of net chemical production in the assimilation model should not dramatically impact our conclusions.

4. Comparison of Observations with MERRA-2

In this section, the results of the comparisons between MERRA-2 and observations from ozonesondes and FTIR retrievals during SSWs are discussed. Ground-based observations provide an excellent baseline to assess climate models and assimilated models. However, the use of ground-based observations to directly study the impact of SSWs is challenging because of the sparse site locations, coarse time resolution (ozonesondes), and limited clear-sky conditions and sunlight (FTIR). In this study, we take advantage of a dense network of observations to assess the performance of MERRA-2. The use of MERRA-2 allows us to investigate the fluctuations over

https://doi.org/10.5194/acp-2021-646
Preprint. Discussion started: 25 August 2021


Atmospheric Chemistry and Physics Discussions

the entire Arctic with consistent temporal and spatial resolution. To visualize the observation frequency and the overall performance of MERRA-2, the time series of PCO from MERRA-2 3-hourly data and ozonesondes and FTIR from winter 2007 to spring 2009 are shown in Figure 2. Two major SSWs occurred during this time period. To exhibit a consistent time series and to avoid the impact of the variability of maximum height of the ozonesondes, PCO from the ground to 20 km is shown. Figure 2 shows the high temporal frequency of the FTIR retrievals compared to ozonesondes during polar day, the consistent frequency of ozonesondes throughout the year, and the gap in solar FTIR retrievals at high latitudes during polar night. The results indicate a good overall agreement of MERRA-2 with observations. The sparsity of FTIR ozone retrievals at Thule in 2008 was due to instrument issues. To have a more clear understanding of the uncertainties in MERRA-2 estimations, more quantitative comparisons are needed.

To investigate the uncertainties of MERRA-2 ozone data during the highly anomalous conditions during SSWs and to consider the enduring impact of SSWs on trace gases, comparisons are performed from 1 December to 1 May for all six events. The results of comparisons between ozonesondes and MERRA-2 are depicted in Figure 3. The mixing ratios from the ozonesonde profiles are subtracted from the MERRA-2 profiles and divided by the ozonesonde concentration at the corresponding levels and are shown as the difference ratios. The mean and standard deviation of the difference ratios in three layers PCO [ground to 5km (G-5km), 5km-10km, 10km-30km], are also reported in Figure 3. The PCO difference ratio is estimated as PCO from MERRA-2 minus ozonesonde PCO divided by ozonesonde PCO for each of the 3 layers. These layers indicate different performance of MERRA-2 by height and show the effect of atmospheric pressure on the contribution of each level to the total ozone column. The G-5km layer includes the troposphere, the 5km-10km includes upper troposphere-lower stratosphere (UTLS), while the 10-30km layer includes the middle and lower stratosphere. The partial column is calculated only up to the altitude of the balloon burst of the ozonesonde, if the burst height is below 30 km.

Large difference ratios between MERRA-2 and the ozonesondes near the surface indicate a well-defined high bias in MERRA-2 at Ny-Alesund and Eureka. The occasional extreme low ozone mixing ratios observed in the lower atmosphere and near the surface are linked to catalytic

https://doi.org/10.5194/acp-2021-646
Preprint. Discussion started: 25 August 2021


Atmospheric Chemistry and Physics Discussions

reactions involving bromine. This chemical ozone depletion is more common at Arctic sites near the ocean (Tarasick and Bottenheim, 2002). MERRA-2 is shown to be unable to retrieve the extreme low ozone values near the surface.

Overall, the variability of the difference ratios at lower altitudes are larger (Figure 3). Ny-Alesund and Eureka show 5%(±23%) and 18%(±26%) mean (±std) difference ratio at G-5km. However, the G-5km layer, on average, contains less than 20 DU, which is less than 6% of total column ozone (TCO). PCO of the G-5 km layer is only 1.5% of TCO at Summit Station where the site elevation is 3.2 km. The PCO difference ratio at Summit station shows very small bias with a standard deviation of ±15%.

The positive bias decreases higher in the troposphere, and the scatter plot shows negative difference ratios. From 5 km to 10 km, a non-significant (higher standard deviation) negative mean bias exists at all sites. The mean PCO difference ratios from 5 km to 10km are -8%(±13%), -15%(±15%), and -8%(±16%) at Summit Station, Ny-Alesund, and Eureka.

The MERRA-2 ozone data between 10 and 30 km are highly correlated with the ozonesondes with $R^2 > 90\%$ (not shown). From 10 to 15 km, the difference ratios are slightly positive and, above 15 km, a negligible bias and low standard deviations are observed. The mean PCO difference ratio in the 10-30 km layer is equal to or less than 3% (±7%) at all stations. The differences between 10 and 30 km are more impactful in TCO uncertainty analysis because this region contains most of the column ozone. (The average PCO for each layer is reported in Figure 3.)

Figure 4 summarizes the comparison between the MERRA-2 and the FTIR retrievals for December 1st to May 1st for all six SSW years. The partial column comparisons for ground to 8 km, 8-15 km, 15-22 km, and 22-34 km are shown. Here the partial columns are defined based on the averaging kernel of the NDACC retrievals. The mean and standard deviation of difference ratios, the mean PCO for each layer are shown in Figure 4.

https://doi.org/10.5194/acp-2021-646
Preprint. Discussion started: 25 August 2021


Atmospheric Chemistry and Physics Discussions

The layers between 15-22 km and 22-34 km contain the most column ozone with averages of 146 DU and 101 DU, respectively. MERRA-2 and the FTIR retrievals have good agreement in these layers with difference ratios of -2%±5% and -4%±5%, respectively.

In the lowest layer, the differences are the largest with a standard deviation ratio of higher than 15% at all stations and mean differences in the range of -7% to 3%. Large differences are observed between 8-15 km, where MERRA-2 estimates 7%-13% more ozone than the FTIR retrievals, and the standard deviations are large. Large differences and standard deviations below 15 km indicate that higher uncertainties exist in both the FTIR retrievals and the MERRA-2 estimation.

In conclusion, when compared to observations, MERRA-2 captures large fluctuations in middle stratospheric ozone at high northern latitudes during winters and early spring that are impacted by SSWs. However, the differences in the lower stratospheric and tropospheric layers exhibit larger values. The higher uncertainties below 15 km during the five months impacted by SSWs are consistent with higher uncertainties in MERRA-2 in these layers year-round, as seen in previous studies (Gelaro et al., 2017; Wargan et al., 2017). The agreement between MERRA-2 ozone with observations during SSWs motivates the use of MERRA-2 dataset to further understand the mid-stratospheric ozone fluctuations during SSWs. The maximum height of ozonesondes is around 30-35 km and ground-based remote sensing loses sensitivity with increasing altitude, thus this study cannot improve previous research on upper stratosphere where higher uncertainties were reported compared to the mid stratosphere. Because more than 75% of ozone molecular density exists in the middle stratosphere (15 to 30 km), the total column uncertainty is dominated by uncertainties in mid-stratospheric layers. In the following section, we discuss ozone variability in the total column and the vertical profile up to 60 km, while our primary analysis is focused on the mid-stratospheric layers because this is where the measurements are most reliable which also has the dominant density of ozone.

https://doi.org/10.5194/acp-2021-646
Preprint. Discussion started: 25 August 2021


Atmospheric Chemistry and Physics Discussions

5. SSWs and their impact on ozone

Disturbances in stratospheric circulation have an impact on stratospheric trace gas concentrations. Consequently, the temporal changes of trace gas concentrations can provide a better understanding of atmospheric circulation including vertical and horizontal transport (Manney et al., 2009a). In this section, the impact of altered circulation patterns on ozone is analyzed, and by investigating the evolution of polar vortex and temperature more detailed characterization of ozone variability is provided.

To understand the rapid alteration of ozone and the average position of the polar vortex before and after each SSW, the anomaly of total column ozone (TCO) and the average Ertel's potential vorticity (PV) contours of 60 and 80 (105 K m2 Kg-1 s-1) at isentropic level with the potential temperature of 850 K for 15 days preceding and 15 days after each of SSWs are shown in Figure 5. In the following parts the main characterization of each SSWs, the evolution of polar vortex, and TCO changes are discussed.

2006: On 21 January 2006, the second strongest and prolonged major SSW since 2004 was detected (Table 2, Siskind et al., 2007; Manney et al., 2008b; 2009a). The easterly zonal mean zonal wind lasted 26 days. Prior to the major SSW, a minor SSW was detected on 9 January (Manney:2008b, Manney:2009a). The polar vortex moved toward Siberia and receded away from Greenland during the minor warming. The polar vortex then displaced westward and equatorward toward northwestern Europe before the major SSW as shown in Figure 5a.

2008: The dynamical circulation was quite variable during winter 2008. Two minor SSWs in mid and late January and one major SSW in late-February are recorded in 2008 (Goncharenko and Zhang, 2008; Flury et al., 2009; Thurairajah et al., 2010; Korenkov et al., 2012). The easterly winds lasted 15 days during the major warming on 22 February. This event is recorded as the latest in the winter season and the least prolonged among the six SSWs considered in this study (Table 2). The polar vortex is displaced mostly over northwest Europe during the development of the SSW in 2008 as shown in Figure 5c. The polar vortex displacement over Europe led to ozone

https://doi.org/10.5194/acp-2021-646
Preprint. Discussion started: 25 August 2021


Atmospheric Chemistry and Physics Discussions

depletion and the enhancement of stratospheric water vapor over northern Europe by mid-February (Flury et al, 2009).

2009: Following an undisturbed and cold early winter, the strongest and most persistent SSW among this study events occurred on 2 January 2009 as shown in Table 2 (Manney et al., 2009b; Harada et al., 2010; Lee and Butler, 2019). The extended elongated shape of the polar vortex before the SSW can be seen in Figure 5e, which resulted in a split vortex. The prolonged SSW in late January recorded 30 days of easterlies at 10 hPa with a maximum magnitude of 29 m/s (Table 2).

2013: The atmospheric disruption associated with the major SSW on 6 January 2013 displaced the polar vortex toward Europe (Figure 5g) and eventually caused the stratospheric polar vortex to split and smaller vortices to appear over Canada and Siberia in mid to late January (Manney et al., 2015). The isolated, offspring vortex lasted for more than two weeks over Canada as shown in Figure 5h.

2018: A major SSW was detected on 12 February 2018. However, the disturbed circulation started in January, with 8 days of zonal wind deceleration occurring in mid-January (Rao et al., 2018). The elongated pattern of PV contours from Europe to eastern Canada shown in Figure 5i indicates a highly disturbed vortex prior to the major SSW and finally led to the vortex split (Karpechko et al., 2018; Rao et al., 2018; Butler et al. 2020). The split vortices were located over Canada/northwest US and northwestern Europe and lasted for almost a week after the detected SSW. The signal of the offspring vortex after the SSWs over Canada is visible in Figure 5j. The major SSW and its associated polar vortex dispersal caused record-breaking cold surface temperatures in northwest Europe (Greening and Hodgson, 2019).

2019: The major SSW on 2 January 2019 (Butler et al. 2020; Rao et al., 2019, Schranz et al., 2020) is the earliest in the winter season and weakest in the magnitude of reversal among the most recent six events studied here (Table 2). The polar vortex was displaced toward Europe before the major SSW occurred (Figure 5k). The continuous wave activity caused a vortex displacement

https://doi.org/10.5194/acp-2021-646
Preprint. Discussion started: 25 August 2021


Atmospheric Chemistry and Physics Discussions

to be followed by a split vortex. The resulting vortices were located over the northeastern US and northwestern Europe as shown in Figure 5l.

As shown in Figure 5, the vortex displacement toward the southeast (Europe) prior to the major SSW as seen in 2006, 2008, 2013, and 2019 (hereafter the displaced vortex SSWs) caused an early positive ozone anomaly in the region outside of the vortex which includes parts or all of the north pole, high latitude in North America, eastern Siberia, and Greenland sector. After the vortex breakdown, the geographical extent of the positive ozone anomalies is mostly limited to high latitudes with a semi-symmetrical shape in these cases. On the other hand, an elongated polar vortex prior to the major SSW as seen in 2009 and 2018 (hereafter the elongated vortex SSWs) is associated with negative ozone anomalies over a large extent of high latitudes, followed by strongly positive TCO anomalies over an extensive area after vortex breakdown.

To investigate the connection of polar vortex strength and TCO, the scatter plot of the zonally averaged EPV change at the potential temperature of 850 K versus the corresponding change in TCO is shown in Figure 6. The ratio of change for each variable is estimated as the average of 15 days after SSWs subtracted by the average of 15 days before the SSWs and divided by the average of 15 days before the SSWs. A correlation between the magnitude of change in EPV and TCO is evident. The elongated vortex SSWs (2009 and 2018) exhibit a higher magnitude of change in both EPV and TCO in this period. It should be noted that making statistical conclusions out of six SSWs is not the intention of this analysis, however, these observations motivate further analysis of this study and future ones.

As the Greenland sector is one of the critical regions that exhibits positive ozone anomalies before the displaced vortex SSWs, negative ozone anomalies before the elongated polar vortex, and strong positive ozone anomalies after the vortex break down, the ozone variability over the Greenland sector (60ºN to 80ºN and 10ºW to 70 ºW) as well as the zonal average (60ºN to 80ºN) is analyzed to investigate the similarities and differences of the impacts of SSWs on zonal and regional high latitude ozone. The structure of ozone anomalies in the zonal minus Greenland sector is similar to the zonal average, therefore it is not included in further analysis. The Greenland sector

https://doi.org/10.5194/acp-2021-646
Preprint. Discussion started: 25 August 2021


Atmospheric Chemistry and Physics Discussions

has been shown to be uniquely sensitive to dynamical forcing associated with the Quasi-Biennial Oscillation (QBO) (Anstey and Shepherd, 2014; Bahramvash-Shams et al., 2019). Moreover, the Greenland sector exhibits a very strong isolated stratospheric air circulation during wintertime, as shown by the climatology of the polar vortex and its associated minimum temperature in Figure 1. Thus, it is important to understanding the regional impact of SSWs on the Greenland sector.

To track the strength of the polar vortex, the average PV at the potential temperature of 850 K over the zonal average and the Greenland sector during 40 days before to 60 days after each SSW is shown in the first column of Figure 7 The evolution of TCO over the zonal average and the Greenland sector is shown in the second column of Figure 7. The climatologies of PV and TCO for both the zonal average and Greenland sectors in Figure 7 are estimated based on non-SSWs years between 2004 to 2019. To quantify the influence of SSWs on ozone, the average TCO for the period spanning 40 days before to 60 days after the SSWs are shown in the bottom right of each plot, as well as the ratio of the changes.

The climatological polar vortex position is located over the Greenland Sector (Figure 1) and explains the higher intensity of climatological EPV over the Greenland sector compared to the zonal climatology in Figure 7. The impact of minor SSWs in 2006 (around lag -25 and -19) and in 2008 (lag -30 and -15), as well as sudden polar vortex displacement to Eurasia in 2019 (lag -20) showed a stronger signal on the averaged EPV over the Greenland sector by larger drop in EPV compared to the zonal. The duration of the polar vortex recovery is defined by the number of days between the date of the SSW and the date in which the zonal EPV returns to its climatological value, as reported in the last column of Table 2. The fastest recovery of 30 days is observed in 2019 (also the weakest SSW) and the longest recovery duration of around 45 days is observed in 2009, 2013, and 2018. The recovery duration is similar with only a few days difference if the EPV over the Greenland sector is used instead.

Compared to the 40-day average of TCO prior to the SSW, the highest percent zonal TCO increase is observed for one of the elongated polar vortex SSWs with 29% in 2009. The maximum percent TCO increases over the Greenland sector belong to both elongated polar vortex SSWs with

https://doi.org/10.5194/acp-2021-646
Preprint. Discussion started: 25 August 2021


Atmospheric Chemistry and Physics Discussions

37% in 2018 and 31% in 2009. In all SSWs the magnitude of percent increased TCO is higher over the Greenland sector compared to the zonal average with the exception of 2006, due to the effects of the minor warming and a long period of high positive ozone anomalies over the Greenland sector before the SSW.

The zonal TCO in half of the studied SSWs (2006, 2009, and 2013) does not get back to the climatological TCO within two months after the SSWs, however, over the Greenland sector the TCO reached the climatology in 30, 47, and 50 days respectively. In the other 3 SSWs the TCO over Greenland returned to the climatology a few days before the zonal average. Therefore, on average, the TCO over the Greenland sector shows a faster recovery and returns to climatological levels within 25 to 55 days after the event as shown in Figure 7. No distinct pattern is observed in elongated (2009, 2018) vs displaced vortex SSWs in regard to the recovery to the climatological TCO.

Analyzing the vertical structure of ozone provides more details of the impact of SSWs. Figure 8 shows the temporal evolution of the vertical structure of ozone as a cross-section of the ozone anomalies for both the zonal average and the Greenland sector from 40 days before to 60 days after each SSW. The positive ozone anomaly in mid stratospheric layers (15 to 30km) starts from a few weeks (15 to 25 days) prior to the displaced vortex SSWs (2006, 2008, 2013, and 2019) over both the zonal average and the Greenland sector. The negative ozone anomalies 15 days before the SSWs and extreme positive ozone after the SSWs in mid stratospheric layers for the two elongated vortex SSWs (2009, 2018) are evident. The enduring impact of SSWs on ozone in different atmospheric layers is clear in all cases and shows a similar pattern for both the zonal averaged and the Greenland sector, as expected the structures of ozone anomalies are smoother in the zonal average compared to the Greenland sector compared as shown in Figure 8. More intense and frequent negative ozone anomalies in mid stratospheric layers at the end of study period is also reflected by the faster recovery of TCO to climatological values as shown in Figure 7. The shortest impact on TCO belongs to 2008 because of multiple disturbances in the circulation and the shortest duration of easterlies (Table 2).

https://doi.org/10.5194/acp-2021-646
Preprint. Discussion started: 25 August 2021


Atmospheric Chemistry and Physics Discussions

To highlight the temperature variation, Figure 9 shows the cross-section of the temperature anomaly for the zonal average from 40 days before to 60 days after each SSW. Figure 9 focuses only on the zonal average, as the anomaly of temperature profile had similar patterns over the zonal and the Greenland sectors. The positive temperature anomalies in mid stratospheric layers start a few weeks before the SSWs in the 4 cases of a displaced vortex (2006, 2008, 2013, and 2019). On the other hand, the intrusion of the positive temperature anomalies to mid stratospheric layers is almost coincident with SSWs in the 2 elongated vortex cases. The duration of positive temperature anomalies in mid stratospheric layers is 10 days to 30 days shorter than ozone positive anomalies (Figure 8 and Figure 9). The positive temperature anomaly is more persistent at lower levels of the stratosphere, where the enduring impact of SSWs on mid-stratosphere ozone (up to 25 -30 km) is clear in all of the SSWs studied here.

6. Discussion

The cyclonic polar vortex during wintertime is generated in response to the seasonality of radiative cooling. The intensified wave forcing before the SSW is manifested by both accelerated tropical upwelling and polar downwelling, which leads to advection of low EPV air parcels poleward. The conservation of EPV causes anticyclonic circulation, which gradually drives easterly zonal mean zonal winds, and leads to displacement or splitting of the polar vortex. The resultant reduction in the vorticity induces strong descent and consequently an adiabatic temperature increase in the stratosphere (Matsuno, 1971; Limpasuvan et al., 2012).

Here the MERRA-2 dataset is used to determine the impact of the dynamical terms during each SSW. Because of the constraints in tracer continuity estimation using equation (2), these analyses are estimated over the Arctic zonal average only and not the Greenland sector. The vertical component of the residual circulation ($\overline{w}^*$) as defined in equation (3) is an indicator of wave forcing. The cross-section of the vertical component of residual circulation during 40 days prior to and 60 days after the SSW over the zonal average (60ºN to 80ºN) is shown in Figure 10. More intense downward propagation is shown as darker blue. The increased wave forcing preceding the SSW is evident in Figure 10 with negative $\overline{w}^*$ anomalies, which indicate strong

https://doi.org/10.5194/acp-2021-646
Preprint. Discussion started: 25 August 2021


Atmospheric Chemistry and Physics Discussions

downwelling in the zonal average. Occurrences of minor SSWs are evident by the early appearance of increased wave forcing, as seen in 2006 and 2008. A very intense and abrupt increase in downward propagation was observed in 2009. Disturbed circulations in the middle stratosphere before the SSWs are seen in 2018 and 2019 (lag -30 to -20).

Following the SSW, residual circulation is weakened as shown in Figure 10. The intensity of increased wave activity is reduced shortly after the SSW. However, the decrease in wave activity is gradual, in general, and lasts a few weeks as shown in Figure 10. The suppressed wave activity creates preferable conditions for the recovery of the zonal mean zonal wind, temperature, and ozone. Shortly after the SSW, the recovery starts in the upper stratosphere as shown in Figure 9. However, different radiative relaxation time scales cause a slower recovery in the lower stratosphere compared to upper stratospheric layers (Dickinson, 1973; Randel et al., 2002; Hitchcock and Simpson, 2014). The dynamical alteration suppresses any further upward propagation of the planetary waves, which explains the descending pattern of temperature up to weeks after the SSW (Matsuno, 1971).

The impact of each term in tracer continuity (equation (2)) on ozone for each SSW are investigated and shown in Figure 11. The composite effect of chemistry during SSWs is important in the upper stratosphere (de la Cámara et al 2018b). The analysis of dynamical parameters in this study are limited to 30 km to minimize the impact of chemical processes. The cross-section of ozone tendency (dO_3/dt, left side of equation (2)), the horizontal component of eddy mixing $e^{(z/H)}(M_y/dy)$ (M_y as defined in equation(4)), the vertical component of eddy mixing $e^{(z/H)}(M_z/dz)$ (M_z as defined in equation(5)), the horizontal advection transport (the first term on the right side of equation (2)), vertical advection transport (the second term on the right side of equation (2)), and summation of right side equation(2) (called the estimated ozone tendency) during the 40 days prior to and 60 days after the SSW over the zonal average are shown in Figure 11.

The estimated ozone tendency (last column of Figure 11) shows that using MERRA-2 fields, dynamical terms of tracer continuity can simulate the main features of the observed ozone tendency (first column of Figure 11) below 30 km and use these estimates to investigate the impact

https://doi.org/10.5194/acp-2021-646
Preprint. Discussion started: 25 August 2021


Atmospheric Chemistry and Physics Discussions

of different terms of tracer continuity on ozone. The key role of vertical advection and horizontal eddy mixing on ozone tendency is evident in Figures 11. Vertical advection is the main driver of ozone tendency in the mid stratosphere. Intensified residual circulation (Figure 10) dramatically impacts the ozone increase. A significant signal of vertical advection is evident from 10 to 30 km in all six SSWs and is coincident with enhanced wave activity (Figure 10), which is magnified around SSWs; however, it persists well after the vertical residual circulation signal disappears, up to two months after the SSWs. The sudden and intensified vertical advection is more magnified in 2009 and 2018 with an enduring elongated polar vortex.

Horizontal eddy mixing is the second important contributor in ozone tendency over the mid stratosphere. While vertical advection builds up the ozone tendency, horizontal mixing tends to balance and weaken the ozone tendency. Increased wave activity and large-scale mixing influence a prolonged enhancement of the diffusivity of PV flux, which leads to increased horizontal eddy transport (Nakamura, 1996; de la Cámara et al., 2018a; 2018b). Vertical eddy mixing has a clear signal above 20 km during minor and major SSWs. Horizontal advection has the least significant contribution to ozone tendency. The dominant contribution of vertical advection on mid-stratospheric ozone variability (15 to 30 km) using MERRA-2 dynamic parameters are consistent with climate model analysis (Tao et al., 2015; de la Cámara et al., 2018b). Considering the larger uncertainties of ozone estimation in MERRA-2 below 15 km, and the possibility of larger uncertainties in dynamic parameter estimations, this study does not analyze the impact of the dynamics on ozone in the lower stratosphere. Using climate models, it has been shown that the horizontal eddy mixing term plays a key role in the ozone variability in the lower stratosphere during the SSWs (de la Cámara et al., 2018b).

The time series of vertically integrated (15 to 30 km) ozone tendency, horizontal eddy mixing, vertical advection, and the residual of tracer continuity considering all terms in equation (2) are shown in Figure 12. The major contribution of vertical advection on ozone tendency is evident in Figure 12. The higher intensity of ozone tendency and vertical advection and their strong correlation coincident with the SSW date of the elongated polar vortex (2009 and 2018) stand out in Figure 12.

https://doi.org/10.5194/acp-2021-646
Preprint. Discussion started: 25 August 2021


Atmospheric Chemistry and Physics Discussions

Although the estimated ozone tendency (last column in Figure 11) simulates most features of the observed ozone tendency (the first column in Figure 11), they are not identical. The vertically integrated difference in observed and estimated ozone tendency is shown as the residual. The residual of tracer continuity results from both the numerical approximation of terms in equation (2) (errors in the vertical derivatives over high latitude can be large as cos(φ) gets small) as well as the uncertainties in the balance of dynamical parameters in the reanalysis due to the data assimilation process (Martineau et al. 2018). Also, the possibility of chemical processes during splitting or displacement of the polar vortex out of the polar night region might contribute to the residual of tracer continuity. It should be noted that when viewing individual events, the plots are expected to be noisier than the average of numerous events.

7. Conclusion

SSWs are a major manifestation of disturbed stratospheric circulations. The altered dynamics influence the cycle of trace gases including ozone. MERRA-2 reanalysis is used to investigate the influence of six recent SSWs on ozone for the zonal average at high latitudes (60ºN to 80ºN).

The comparison of the MERRA-2 ozone dataset with a unique density of observations at high latitudes from 2004 to 2020 provides an update to previous evaluations and provides understanding of the performance of MERRA-2 during high variability associated with extreme dynamical events such as SSWs. Comparisons are applied during December to May for each SSW. MERRA-2 shows good agreement with ozonesondes and FTIR observations in the middle stratosphere during highly altered dynamics of SSWs.

Comparison with ozonesondes at three high latitude locations showed the mean difference ratio of 3% (±7%) in the stratosphere layer (10-30 km). However, the uncertainties are larger from the ground to 10 km. From 5km to 10km, a non-significant (higher standard deviation) negative mean bias exists in all sites (-8% to 15%). The highest standard deviation of difference ratios is

https://doi.org/10.5194/acp-2021-646
Preprint. Discussion started: 25 August 2021


Atmospheric Chemistry and Physics Discussions

observed at G-5 km (<20%). A positive bias is observed at surface levels where observations show depleted ozone due to bromine reactions.

Using a smoothing method, MERRA-2 is compared to five NDACC FTIR sites in four vertical layers (ground-8km, 8-15km, 15-22km, and 22-30km) during SSWs. These layers are defined based on the sensitivity of FTIR sensors. Overall, higher uncertainties are observed at the lowest level with 18% std. The best agreement is observed between 15-22 km and 22-34 km with -2%(±5%) and -4%(±5%) mean(std) difference ratios. These results emphasize the high quality of MERRA-2 and motivate its usage in mid stratospheric ozone analysis at high northern latitudes during highly disturbed dynamical events. Higher uncertainties in UTLS are also expected because MLS has lower sensitivity at lower altitudes and the dominant contribution of MLS in MERRA-2 reanalysis. Moreover, this study emphasizes the importance of independent ozone observations, such as ozonesondes and FTIR retrievals, as a means to evaluate models and assimilation estimations around the globe.

Using the MERRA-2 dataset, the variability of ozone during the SSWs and associated dynamic parameters are investigated. The evolution of the polar vortex and its impact on the ozone variability is studied using the average EPV at the potential temperature of 850 K. We identify two different patterns in the polar vortex before the SSWs and the subsequent impact on ozone. In 2009 and 2018, an elongated polar vortex is observed before the SSWs which caused a dominant-negative ozone anomaly at northern high latitudes and is followed by an extensive positive ozone anomaly with large geographical extent. The TCO increases rates and the magnitude of change in EPV after these cases are large and the intrusion of positive temperature anomalies to the mid stratosphere is coincident with SSWs date.

During the SSWs in 2006, 2008, 2013, and 2019, the polar vortex is displaced towards Europe, and the TCO exhibits positive anomalies before the SSWs in a large geographical region of northern high latitudes (outside the polar vortex). The positive TCO anomalies after the SSW have a smaller extent, and the magnitude of TCO variability and EPV change is smaller compared

https://doi.org/10.5194/acp-2021-646
Preprint. Discussion started: 25 August 2021


Atmospheric Chemistry and Physics Discussions

to observed changes during the elongated vortex event as seen in 2009 and 2018. The positive temperature anomalies in the middle stratosphere appear a few weeks before the SSW.

A strong relation is observed between the magnitude of change in the averaged EPV 15 days after compared to 15 days before the SSW and the magnitude of TCO change for the same period for all six studied SSWs.

The Greenland sector is one of the critical regions that is impacted by negative TCO before the elongated polar vortex in 2009 and 2018; positive TCO occurs before displaced SSWs. To identify the similarities and differences of zonal versus the regional impact of SSWs on ozone, the analyses are applied over the Greenland sector as well as the zonal average. The general structure of the vertical ozone anomaly over the Greenland sector is similar to the zonal. However, as expected the ozone anomaly over the zonal average is smoother than the Greenland sector which results in a more magnified TCO increase over Greenland. The increased rate over the Greenland sector is between 15% in 2006 to 38% in 2018, while the zonal average ranges between 8% in 2008 to 29% in 2009. Moreover, TCO exhibits a faster recovery to the climatology values over this region compared to the zonal average.

We examined the dynamical terms associated with ozone tendency and investigated the evolution of ozone variability for each SSW using MERRA-2. The main features of observed ozone tendency are captured by the dynamical terms of the tracer continuity equation up to 30 km using MERRA-2 variables. Vertical advection is shown to be the main contributor of ozone tendency in the middle stratosphere during the SSWs and is more magnified during the enduring elongated polar vortex in 2009 and 2018. The impact of vertical advection coincides with the time of enhanced wave activity but can persist up to two months after the SSWs.

Suppressed wave activity initiates the recovery of temperature and ozone. However, the upper stratosphere experiences a faster recovery compared to the lower stratosphere because of the different radiative relaxation time scales. The faster recovery of zonal temperature and ozone at middle stratosphere within 30 days is recorded for 2008 with the shortest duration easterly zonal mean zonal winds. The zonal TCO did not return to climatological TCO values within two months

https://doi.org/10.5194/acp-2021-646
Preprint. Discussion started: 25 August 2021


Atmospheric Chemistry and Physics Discussions

after the SSWs in 2006, 2009, and 2013. The positive ozone anomaly in the middle stratosphere lasts longer than the positive temperature anomaly in most of the SSWs by 10 days or more.

In conclusion, the MERRA-2 dataset is shown to capture ozone variability in the middle stratosphere and provides dynamical information to investigate the impact of SSWs. The impact of SSWs on ozone and the role of vertical advection is shown to be more intense in 2009 and 2018 with an elongated polar vortex compared to displaced vortex in 2006, 2008, 2013, and 2018. The magnitude of change in ozone is correlated with the magnitude of EPV change during the SSWs. Using a more extended dataset could help to shed light on further details and to create more robust statistics regarding Arctic SSWs. Considering the impact of high latitude ozone on global climate and lower latitude surface temperature, the dramatic ozone increases over high latitudes during SSWs points to consequences of these events on the global earth system and possible environmental/ecosystem changes that could be investigated in future studies.

Acknowledgements

We acknowledge NASA's Global Monitoring and Assimilation Office (GMAO) for providing the Modern-Era Retrospective analysis for Research and Applications, Version 2 (MERRA-2). We acknowledge the Ozone and Water Vapor Group at the Earth System Research Laboratory of the National Oceanic and Atmospheric Administration for use of the ozonesonde data and the science technicians at Summit Station, Greenland for launching the ozonesondes. We acknowledge World Ozone and Ultraviolet Radiation Data Centre (WOUDC) for providing Canadian and Norwegian ozonesondes. We acknowledge the Network for the Detection of Atmospheric Composition Change (NDACC) for providing trace gas retrievals from solar FTIRs. This research was supported by NSF grants PLR-1420932 and PLR-1414314.

References

Ancellet, G., Daskalakis, N., Raut, J. C., Tarasick, D., Hair, J., Quennehen, B., et al. (2016). Analysis of the latitudinal variability of tropospheric ozone in the Arctic using the large number of aircraft and ozonesonde observations in early summer 2008. Atmospheric Chemistry and Physics, 16(20), 13341–13358. http://doi.org/10.5194/acp-16-13341-2016

https://doi.org/10.5194/acp-2021-646
Preprint. Discussion started: 25 August 2021

Atmospheric Chemistry and Physics Discussions

Andrews, D. G., J. R. Holton, and C. B. Leovy (1987), *Middle atmosphere dynamics*, Academic Press, San Diego, California.

Anstey, J. A., and T. G. Shepherd (2014), High-latitude influence of the quasi-biennial oscillation, *Quarterly Journal of the Royal Meteorological Society*, *1*(40), 1–21, doi:10.1002/qj.2132.

Bahramvash-Shams, S., Walden, V. P., Petropavlovskikh, I., Tarasick, D., Kivi, R., Oltmans, S., et al. (2019). Variations in the vertical profile of ozone at four high-latitude Arctic sites from 2005 to 2017. Atmospheric Chemistry and Physics, 19(15), 9733–9751. http://doi.org/10.5194/acp-19-9733-2019

Baldwin, M. P., and T. J. Dunkerton (2001), Stratospheric Harbingers of Anomalous Weather Regimes, *Science*, *294*(5), 581–584, doi:10.1126/science.1063315.

Baldwin, M. P., Ayarzagüena, B., Birner, T., Butchart, N., Butler, A. H., Charlton-Perez, A. J., et al. (2021). Sudden Stratospheric Warmings. Reviews of Geophysics, 59(1), 27.1–37. http://doi.org/10.1029/2020RG000708

Bevis, M., Harig, C., Khan, S. A., Brown, A., Simons, F. J., Willis, M., et al. (2019). Accelerating changes in ice mass within Greenland, and the ice sheet's sensitivity to atmospheric forcing (Vol. 116, pp. 1934–1939). Presented at the Proceedings of the National Academy of Sciences, National Academy of Sciences. http://doi.org/10.1073/pnas.1806562116

Bognar, K., Zhao, X., Strong, K., Boone, C. D., Bourassa, A. E., Degenstein, D. A., et al. (2019). Updated validation of ACE and OSIRIS ozone and NO2 measurements in the Arctic using ground-based instruments at Eureka, Canada. Journal of Quantitative Spectroscopy and Radiative Transfer, 238, 106571. http://doi.org/10.1016/j.jqsrt.2019.07.014

Butler, A. H., L. M. Polvani, and C. Deser (2014), Separating the stratospheric and tropospheric pathways of El Niño–Southern Oscillation teleconnections, *Environ. Res. Lett.*, *9*(2), 024014–10, doi:10.1088/1748-9326/9/2/024014.

Butler, A. H., D. J. Seidel, S. C. Hardiman, N. Butchart, T. Birner, and A. Match (2015), Defining Sudden Stratospheric Warmings, *Bull. Amer. Meteor. Soc.*, *96*(11), 1913–1928, doi:10.1175/BAMS-D-13-00173.1.

Butler, A. H., Sjoberg, J. P., Seidel, D. J., & Rosenlof, K. H. (2017). A sudden stratospheric warming compendium. Earth System Science Data, 9(1), 63–76. http://doi.org/10.5194/essd-9-63-2017

Butler, A. H., and E. P. Gerber (2018), Optimizing the Definition of a Sudden Stratospheric Warming, *J. Climate*, *31*(6), 2337–2344, doi:10.1175/jcli-d-17-0648.1.

Butler, A., Charlton Perez, A., Domeisen, D. I. V., Garfinkel, C., Gerber, E. P., Hitchcock, P., et al. (2019). Sub-seasonal Predictability and the Stratosphere, 223–241. Elsevier Inc. http://doi.org/10.1016/B978-0-12-811714-9.00011-5

https://doi.org/10.5194/acp-2021-646
Preprint. Discussion started: 25 August 2021

Atmospheric Chemistry and Physics Discussions

Butler, A. H., Lawrence, Z. D., Lee, S. H., Lillo, S. P., & Long, C. S. (2020). Differences between the 2018 and 2019 stratospheric polar vortex split events. Quarterly Journal of the Royal Meteorological Society, 146(732), 3503–3521. http://doi.org/10.1002/qj.3858

Cagnazzo, C., and E. Manzini (2009), Impact of the Stratosphere on the Winter Tropospheric Teleconnections between ENSO and the North Atlantic and European Region, *J. Climate*, *22*(5), 1223–1238, doi:10.1175/2008JCLI2549.1.

Calvo, N., L. M. Polvani, and S. Solomon (2015), On the surface impact of Arctic stratospheric ozone extremes, *Environ. Res. Lett.*, *10*(9), 094003–9, doi:10.1088/1748-9326/10/9/094003.

de la Cámara, A., M. Abalos, and P. Hitchcock (2018a), Changes in Stratospheric Transport and Mixing During Sudden Stratospheric Warmings, *J. Geophys. Res.*, *123*(7), 3356–3373, doi:10.1002/2017JD028007.

de la Cámara, A., M. Abalos, P. Hitchcock, N. Calvo, and R. R. Garcia (2018b), Response of Arctic ozone to sudden stratospheric warmings, *Atmospheric Chemistry and Physics*, *18*(22), 16499–16513, doi:10.5194/acp-18-16499-2018.

de la Cámara, A. , T. Birner, and J. R. Albers (2019), Are Sudden Stratospheric Warmings Preceded by Anomalous Tropospheric Wave Activity? *J. Climate*, *32*(21), 7173–7189, doi:10.1175/JCLI-D-19-0269.1.

Charlton, A. J., and L. M. Polvani (2007), A New Look at Stratospheric Sudden Warmings. Part I: Climatology and Modeling Benchmarks, *J. Climate*, *20*(3), 449–469, doi:10.1175/jcli3996.1.

Charlton-Perez, A. J., L. Ferranti, and R. W. Lee (2018), The influence of the stratospheric state on North Atlantic weather regimes, *Quarterly Journal of the Royal Meteorological Society*, *144*(713), 1140–1151, doi:10.1002/qj.3280.

Coy, L., and S. Pawson (2015), The Major Stratospheric Sudden Warming of January 2013: Analyses and Forecasts in the GEOS-5 Data Assimilation System, *Mon. Wea. Rev.*, *143*(2), 491–510, doi:10.1175/MWR-D-14-00023.1.

Coy, L., K. Wargan, A. M. Molod, W. R. McCarty, and S. Pawson (2016), Structure and Dynamics of the Quasi-Biennial Oscillation in MERRA-2, *J. Climate*, *29*(14), 5339–5354, doi:10.1175/JCLI-D-15-0809.1.

Coy, L., S. Eckermann, and K. Hoppel (2009), Planetary Wave Breaking and Tropospheric Forcing as Seen in the Stratospheric Sudden Warming of 2006, *J. Atmos. Sci.*, *66*(2), 495–507, doi:10.1175/2008JAS2784.1.

Dickinson, R. E. (1973), Method of parameterization for infrared cooling between altitudes of 30 and 70 kilometers, *Journal of Geophysical Research*, *78*(21), 4451–4457, doi:10.1029/JC078i021p04451.

https://doi.org/10.5194/acp-2021-646
Preprint. Discussion started: 25 August 2021

Atmospheric Chemistry and Physics Discussions

Flury, T., K. Hocke, A. Haefele, N. Kämpfer, and R. Lehmann (2009), Ozone depletion, water vapor increase, and PSC generation at midlatitudes by the 2008 major stratospheric warming, *J. Geophys. Res.*, *114*(D18), 7903–14, doi:10.1029/2009JD011940.

Fritts, D. C., and M. J. Alexander (2003), Gravity wave dynamics and effects in the middle atmosphere, *Reviews of Geophysics*, *41*(1), 1003, doi:10.1029/2001RG000106.

Fusco, A. C., and M. L. Salby (1999), Interannual Variations of Total Ozone and Their Relationship to Variations of Planetary Wave Activity, *J. Climate*, *12*(6), 1619–1629, doi:10.1175/1520-0442(1999)012<1619:ivotoa>2.0.co;2.

García, O. E., M. Schneider, A. Redondas, Y. González, F. Hase, T. Blumenstock, and E. Sepúlveda (2012), Investigating the long-term evolution of subtropical ozone profiles applying ground-based FTIR spectrometry, *Atmos. Meas. Tech.*, *5*(11), 2917–2931, doi:10.5194/amt-5-2917-2012.

Gaudel, A., G. Ancellet, and S. Godin-Beekmann (2015), Analysis of 20 years of tropospheric ozone vertical profiles by lidar and ECC at Observatoire de Haute Provence (OHP) at 44°N, 6.7°E, *Atmospheric Environment*, *113*(C), 78–89, doi:10.1016/j.atmosenv.2015.04.028.

Gelaro, R., McCarty, W., Suárez, M. J., Todling, R., Molod, A., Takacs, L., et al. (2017). The Modern-Era Retrospective Analysis for Research and Applications, Version 2 (MERRA-2). Journal of Climate, 30(14), 5419–5454. http://doi.org/10.1175/JCLI-D-16-0758.1

Goncharenko, L., and S.-R. Zhang (2008), Ionospheric signatures of sudden stratospheric warming: Ion temperature at middle latitude, *Geophys. Res. Lett.*, *35*(21), L15804–4, doi:10.1029/2008GL035684.

Greening, K., and A. Hodgson (2019), Atmospheric analysis of the cold late February and early March 2018 over the UK, *Weather*, *74*(3), 79–85, doi:10.1002/wea.3467.

Haigh, J. D. (1994), The role of stratospheric ozone in modulating the solar radiative forcing of climate, *Nature*, *370*(6), 544–546, doi:10.1038/370544a0.

Hitchcock, P., and I. R. Simpson (2014), The Downward Influence of Stratospheric Sudden Warmings*, *J. Atmos. Sci.*, *71*(10), 3856–3876, doi:10.1175/JAS-D-14-0012.1.

Holton, J. R., and R. S. Lindzen (1972), An Updated Theory for the Quasi-Biennial Cycle of the Tropical Stratosphere, *J. Atmos. Sci.*, *29*(6), 1076–1080, doi:10.1175/1520-0469(1972)029<1076:autftq>2.0.co;2.

Holton, J. R., P. H. Haynes, M. E. McIntyre, A. R. Douglass, R. B. Rood, and L. Pfister (1995), Stratosphere-troposphere exchange, *Reviews of Geophysics*, *33*(4), 403–439, doi:10.1029/95RG02097.

Houghton, J. T. (1978), The stratosphere and mesosphere, *Q. J. R. Meteorol. Soc.*, *104*, 1–29, doi:doi.org/10.1002/qj.49710443902.

https://doi.org/10.5194/acp-2021-646
Preprint. Discussion started: 25 August 2021

Atmospheric Chemistry and Physics Discussions

Ineson, S., and A. A. Scaife (2008), The role of the stratosphere in the European climate response to El Niño, *Nature Geoscience*, *2*(1), 32–36, doi:10.1038/ngeo381.

Johnson, B. J., S. J. Oltmans, H. Vömel, H. G. J. Smit, T. Deshler, and C. Kröger (2002), Electrochemical concentration cell (ECC) ozonesonde pump efficiency measurements and tests on the sensitivity to ozone of buffered and unbuffered ECC sensor cathode solutions, *J. Geophys. Res.*, *107*(D19), 7881, doi:10.1029/2001JD000557.

Karpechko, A. Y., A. Charlton Perez, M. Balmaseda, N. Tyrrell, and F. Vitart (2018), Predicting Sudden Stratospheric Warming 2018 and Its Climate Impacts With a Multimodel Ensemble, *Geophys. Res. Lett.*, *45*(24), 2096–9, doi:10.1029/2018GL081091.

Karpechko, A. Y., J. Perlwitz, and E. Manzini (2014), A model study of tropospheric impacts of the Arctic ozone depletion 2011, *J. Geophys. Res.*, *119*(1), 7999–8014, doi:10.1002/2013JD021350.

Kidston, J., A. A. Scaife, S. C. Hardiman, D. M. Mitchell, N. Butchart, M. P. Baldwin, and L. J. Gray (2015), Stratospheric influence on tropospheric jet streams, storm tracks and surface weather, *Nature Geoscience*, 1–8, doi:10.1038/ngeo2424.

Knowland, K. E., L. E. Ott, B. N. Duncan, and K. Wargan (2017), Stratospheric Intrusion-Influenced Ozone Air Quality Exceedances Investigated in the NASA MERRA-2 Reanalysis, *Geophys. Res. Lett.*, *44*(20), 10,691–10,701, doi:10.1002/2017GL074532.

Komhyr, W. D. (1986), Operations handbook-ozone measurements to 40-km altitude with Model 4A Electrochemical Concentration Cell (ECC) ozonesondes (used with 1680-MHz radiosondes).

Korenkov, Y. N., Klimenko, V. V., Klimenko, M. V., Bessarab, F. S., Korenkova, N. A., Ratovsky, K. G., et al. (2012). The global thermospheric and ionospheric response to the 2008 minor sudden stratospheric warming event. Journal of Geophysical Research: Atmospheres, 117(A10309). http://doi.org/10.1029/2012JA018018

Lawrence, Z. D., and G. L. Manney (2020), Does the Arctic Stratospheric Polar Vortex Exhibit Signs of Preconditioning Prior to Sudden Stratospheric Warmings? *J. Atmos. Sci.*, *77*(2), 611–632, doi:10.1175/JAS-D-19-0168.1.

Lee, S. H., and A. H. Butler (2019), The 2018–2019 Arctic stratospheric polar vortex, *Weather*, *294*, 581–6, doi:10.1002/wea.3643.

Limpasuvan, V., J. H. Richter, Y. J. Orsolini, F. Stordal, and O.-K. Kvissel (2012), The roles of planetary and gravity waves during a major stratospheric sudden warming as characterized in WACCM, *Journal of Atmospheric and Solar-Terrestrial Physics*, *78-79*(C), 84–98, doi:10.1016/j.jastp.2011.03.004.

Lindzen, R. S., and J. R. Holton (1968), A Theory of the Quasi-Biennial Oscillation, *J. Atmos. Sci.*, *25*(6), 1095–1107, doi:10.1175/1520-0469(1968)025<1095:atotqb>2.0.co;2.

https://doi.org/10.5194/acp-2021-646
Preprint. Discussion started: 25 August 2021

Logan, J. A. (1994), Trends in the vertical distribution of ozone: An analysis of ozonesonde data, *J. Geophys. Res.*, *99*(D), 25–, doi:10.1029/94JD02333.

Logan, J. A., Megretskaia, I. A., Miller, A. J., Tiao, G. C., Choi, D., Zhang, L., Stolarski, R. S., Labow, G. J., Hollandsworth, S. M., Bodeker, G. E., Claude, H., de Muer, D., Kerr, J. B., Tarasick, D. W., Oltmans, S. J., Johnson, B., Schmidlin, F., Staehelin, J., Viatte, P. and Uchino, O., (1999): Trends in the vertical distribution of ozone: A comparison of two analyses of ozonesonde data, J. Geophys. Res., 104(D), 26–, doi:10.1029/1999JD900300.

Manney, G. L., Daffer, W. H., Strawbridge, K. B., Walker, K. A., Boone, C. D., Bernath, P. F., et al. (2008a). The high Arctic in extreme winters: vortex, temperature, and MLS and ACE-FTS trace gas evolution. Atmospheric Chemistry and Physics, 8(3), 505–522. http://doi.org/10.5194/acp-8-505-2008

Manney, G. L., Harwood, R. S., MacKenzie, I. A., Minschwaner, K., Allen, D. R., Santee, M. L., et al. (2009a). Satellite observations and modeling of transport in the upper troposphere through the lower mesosphere during the 2006 major stratospheric sudden warming. Atmospheric Chemistry and Physics, 9(1), 4775–4795. http://doi.org/10.5194/acp-9-4775-2009

Manney, G. L., Krüger, K., Pawson, S., Minschwaner, K., Schwartz, M. J., Daffer, W. H., et al. (2008b). The evolution of the stratopause during the 2006 major warming: Satellite data and assimilated meteorological analyses. Journal of Geophysical Research: Atmospheres, 113(D11), 1576–16. http://doi.org/10.1029/2007JD009097

Manney, G. L., M. J. Schwartz, K. Krüger, M. L. Santee, S. Pawson, J. N. Lee, W. H. Daffer, R. A. Fuller, and N. J. Livesey (2009b), Aura Microwave Limb Sounder observations of dynamics and transport during the record-breaking 2009 Arctic stratospheric major warming, *Geophys. Res. Lett.*, *36*(12), 581–5, doi:10.1029/2009GL038586.

Manney, G. L., Z. D. Lawrence, M. L. Santee, N. J. Livesey, A. Lambert, and M. C. Pitts (2015), Polar processing in a split vortex: Arctic ozone loss in early winter 2012/2013, *Atmospheric Chemistry and Physics*, *15*(10), 5381–5403, doi:10.5194/acp-15-5381-2015.

Marsh, D. R., M. J. Mills, D. E. Kinnison, J.-F. Lamarque, N. Calvo, and L. M. Polvani (2013), Climate Change from 1850 to 2005 Simulated in CESM1(WACCM), *J. Climate*, *26*(19), 7372–7391, doi:10.1175/JCLI-D-12-00558.1.

Martineau, P., Wright, J. S., Zhu, N., & Fujiwara, M. (2018). Zonal-mean data set of global atmospheric reanalyses on pressure levels. Earth System Science Data, 10(4), 1925–1941. http://doi.org/10.5194/essd-10-1925-2018

Martius, O., L. M. Polvani, and H. C. Davies (2009), Blocking precursors to stratospheric sudden warming events, *Geophys. Res. Lett.*, *36*(14), 581–5, doi:10.1029/2009GL038776.

Matsuno, T. (1971), A dynamical model of the stratospheric sudden warming, *J. Atmos. Sci.*, *28*, 1479–1494, doi:https://doi.org/10.1175/1520-0469(1971)028<1479:ADMOTS>2.0.CO;2.

https://doi.org/10.5194/acp-2021-646
Preprint. Discussion started: 25 August 2021

Atmospheric Chemistry and Physics Discussions

McDonald, M. K., D. N. Turnbull, and D. P. Donovan (1999), Steller Brewer, ozonesonde, and DIAL measurements of Arctic O3 column over Eureka, N.W.T. during 1996 winter/spring, *Geophys. Res. Lett.*, *26*(15), 2383–2386, doi:10.1029/1999GL900506.

Molod, A., L. Takacs, M. Suarez, and J. Bacmeister (2015), Development of the GEOS-5 atmospheric general circulation model: evolution from MERRA to MERRA2, *Geosci. Model Dev.*, *8*(5), 1339–1356, doi:10.5194/gmd-8-1339-2015.

Nakamura, N. (1996), Two-Dimensional Mixing, Edge Formation, and Permeability Diagnosed in an Area Coordinate, *Journal of Atmospheric Sciences*, *53*(1), 1524–1537, doi:10.1175/1520-0469(1996)053<1524:TDMEFA>2.0.CO;2.

Nowack, P. J., N. Luke Abraham, A. C. Maycock, P. Braesicke, J. M. Gregory, M. M. Joshi, A. Osprey, and J. A. Pyle (2015), A large ozone-circulation feedback and its implications for global warming assessments, *Nature Clim Change*, *5*(1), 41–45, doi:10.1038/nclimate2451.

Palmeiro, F. M., D. Barriopedro, R. García-Herrera, and N. Calvo (2015), Comparing Sudden Stratospheric Warming Definitions in Reanalysis Data*, *J. Climate*, *28*(17), 6823–6840, doi:10.1175/JCLI-D-15-0004.1.

Polvani, L. M., and D. W. Waugh (2004), Upward Wave Activity Flux as a Precursor to Extreme Stratospheric Events and Subsequent Anomalous Surface Weather Regimes, *J. Climate*, *17*(1), 3548–3554, doi:10.1175/1520-0442(2004)017<3548:UWAFAA>2.0.CO;2.

Ramaswamy, V., M. D. Schwarzkopf, and W. J. Randel (1996), Fingerprint of ozone depletion in the spatial and temporal pattern of recent lower-stratospheric cooling, *Nature*, *382*(6), 616–618, doi:10.1038/382616a0.

Randel, W. J., F. WU, and R. STOLARSKI (2002), Changes in column ozone correlated with the stratospheric EP flux, *Journal of the Meteorological Society of Japan. Ser. II*, *80*, 849–862.

Randel, W. J. (1993), Global variations of zonal mean ozone during stratospheric warming events, *Journal of the Atmospheric Sciences*, 50(19), 3308-3321.

Rao, J., C. I. Garfinkel, H. Chen, and I. P. White (2019), The 2019 New Year Stratospheric Sudden Warming and Its Real-Time Predictions in Multiple S2S Models, *J. Geophys. Res.*, *124*(21), 11155–11174, doi:10.1029/2019JD030826.

Rao, J., R. Ren, H. Chen, Y. Yu, and Y. Zhou (2018), The Stratospheric Sudden Warming Event in February 2018 and its Prediction by a Climate System Model, *J. Geophys. Res.*, *123*(23), 34–14, doi:10.1029/2018JD028908.

Rao, T. N. (2003), Climatology of UTLS ozone and the ratio of ozone and potential vorticity over northern Europe, *J. Geophys. Res.*, *108*(D22), 3451–10, doi:10.1029/2003JD003860.

https://doi.org/10.5194/acp-2021-646
Preprint. Discussion started: 25 August 2021

Atmospheric Chemistry and Physics Discussions

Rao, T. N., J. Arvelius, S. Kirkwood, and P. von der Gathen (2004), Climatology of ozone in the troposphere and lower stratosphere over the European Arctic, *Advances in Space Research*, *34*(4), 754–758, doi:10.1016/j.asr.2003.05.055.

Rienecker, M. M., Suárez, M. J., Gelaro, R., Todling, R., Bacmeister, J., Liu, E., Bosilovich, M. G., Schubert, S. D., Takacs, L., Kim, G.-K., Bloom, S., Chen, J., Collins, D., Conaty, A., da Silva, A., Gu, W., Joiner, J., Koster, R. D., Lucchesi, R., Molod, A., Owens, T., Pawson, S., Pegion, P., Redder, C. R., Reichle, R., Robertson, F. R., Ruddick, A. G., Sienkiewicz, M. and Woollen, J. (2011), MERRA: NASA's Modern-Era Retrospective Analysis for Research and Applications, J. Climate, 24(14), 3624–3648, doi:10.1175/JCLI-D-11-00015.1.

Rodgers, C. D. (2000), *Inverse Methods for Atmospheric Sounding - Theory and Practice*, Series on Atmospheric Oceanic and Planetary Physics, World Scientific Publishing Co. Pte. Ltd.

Rodgers, C. D., and B. J. Connor (2003), Intercomparison of remote sounding instruments, *J. Geophys. Res.*, *108*(D3), n/a–n/a, doi:10.1029/2002JD002299.

Romanowsky, E., D. X. R. Handorf, R. Jaiser, I. Wohltmann, W. Dorn, J. Ukita, J. Cohen, K. Dethloff, and M. Rex (2019), The role of stratospheric ozone for Arctic-midlatitude linkages, *Scientific Reports*, *9*(1), 1–7, doi:10.1038/s41598-019-43823-1.

Rothman, L. S., Gordon, I. E., Barbe, A., Benner, D. C., Bernath, P. F., Birk, M., et al. (2009). The HITRAN 2008 molecular spectroscopic database. Journal of Quantitative Spectroscopy and Radiative Transfer, 110(9-10), 533–572. http://doi.org/10.1016/j.jqsrt.2009.02.013

Scherhag, R. (1952), Die explosionsartigen Stratosparenerwarmungen des Spatwinters, *Ber. Det. Wetterdienstes*, *38*, 51–63.

Schoeberl, M. R. (1978), Stratospheric Warmings: Observations and Theory, *Reviews of Geophysics and Space Physics*, *16*(4), 521–, doi:10.1029/RG016i004p00521.

Scheiben, D., Straub, C., Hocke, K., Forkman, P., & Kämpfer, N. (2012). Observations of middle atmospheric H2O and O3 during the 2010 major sudden stratospheric warming by a network of microwave radiometers. Atmospheric Chemistry and Physics, 12(16), 7753–7765. http://doi.org/10.5194/acp-12-7753-2012

Schranz, F., J. Hagen, G. Stober, K. Hocke, A. Murk, and N. Kämpfer (2020), Small-scale variability of stratospheric ozone during the sudden stratospheric warming 2018/2019 observed at Ny-Ålesund, Svalbard, *Atmospheric Chemistry and Physics*, *20*(18), 10791–10806, doi:10.5194/acp-20-10791-2020.

Scott, R. K., and L. M. Polvani (2004), Stratospheric control of upward wave flux near the tropopause, *Geophys. Res. Lett.*, *31*(2), 581–4, doi:10.1029/2003GL017965.

Shangguan, M., W. Wang, and S. Jin (2019), Variability of temperature and ozone in the upper troposphere and lower stratosphere from multi-satellite observations and reanalysis data, *Atmospheric Chemistry and Physics*, *19*(10), 6659–6679, doi:10.5194/acp-19-6659-2019.

https://doi.org/10.5194/acp-2021-646
Preprint. Discussion started: 25 August 2021

Siskind, D. E., S. D. Eckermann, L. Coy, J. P. McCormack, and C. E. Randall (2007), On recent interannual variability of the Arctic winter mesosphere: Implications for tracer descent, *Geophys. Res. Lett.*, *34*(9), 498–5, doi:10.1029/2007GL029293.

Smit, H. G. J., Straeter, W., Johnson, B. J., Oltmans, S. J., Davies, J., Tarasick, D. W., et al. (2007). Assessment of the performance of ECC-ozonesondes under quasi-flight conditions in the environmental simulation chamber: Insights from the Juelich Ozone Sonde Intercomparison Experiment (JOSIE). Journal of Geophysical Research: Atmospheres, 112(D19), 563–18. http://doi.org/10.1029/2006JD007308

Smith, K. L., and L. M. Polvani (2014), The surface impacts of Arctic stratospheric ozone anomalies, *Environ. Res. Lett.*, *9*(7), 074015–9, doi:10.1088/1748-9326/9/7/074015.

Sterling, C. W., B. J. Johnson, S. J. Oltmans, H. G. J. Smit, A. F. Jordan, P. D. Cullis, E. G. Hall, A. M. Thompson, and J. C. Witte (2017), Homogenizing and Estimating the Uncertainty in NOAA's Long Term Vertical Ozone Profile Records Measured with the Electrochemical Concentration Cell Ozonesonde, *Atmos. Meas. Tech. Discuss.*, 1–39, doi:10.5194/amt-2017-397.

Stolarski, R. S. (2001), History of the Study of Atmospheric Ozone, *Ozone Science Engineering*, *23*(6), 421–428, doi:http://doi.org/10.1080/01919510108962025.

Tao, M., P. Konopka, F. Ploeger, J. U. Grooß, R. Müller, C. M. Volk, K. A. Walker, and M. Riese (2015), Impact of the 2009 major sudden stratospheric warming on the composition of the stratosphere, *Atmospheric Chemistry and Physics*, *15*(15), 8695–8715, doi:10.5194/acp-15-8695-2015.

Tarasick, D. W., and J. W. Bottenheim (2002), Surface ozone depletion episodes in the Arctic and Antarctic from historical ozonesonde records, *Atmospheric Chemistry and Physics*, *2*(3), 197–205.

Tarasick, D. W., J. Davies, H. G. J. Smit, and S. J. Oltmans (2016), A re-evaluated Canadian ozonesonde record: measurements of the vertical distribution of ozone over Canada from 1966 to 2013, *Atmos. Meas. Tech.*, *9*(1), 195–214, doi:10.5194/amt-9-195-2016.

Thurairajah, B., R. L. Collins, V. L. Harvey, R. S. Lieberman, M. Gerding, K. Mizutani, and J. M. Livingston (2010), Gravity wave activity in the Arctic stratosphere and mesosphere during the 2007–2008 and 2008–2009 stratospheric sudden warming events, *J. Geophys. Res.*, *115*(D8), S637–17, doi:10.1029/2010JD014125.

Tiao, G. C., G. C. Reinsel, J. H. Pedrick, G. M. Allenby, C. L. Mateer, A. J. Miller, and J. J. DeLuisi (1986), A statistical trend analysis of ozonesonde data, *J. Geophys. Res.*, *91*(D12), 13121–13136, doi:10.1029/JD091iD12p13121.

Tripathi, O. P., M. Baldwin, A. Charlton-Perez, M. Charron, S. D. Eckermann, E. Gerber, H. R. Harrison, D. R. Jackson, B. M. Kim, Y. Kuroda, A. Lang. S. Mahmood, R. Mizuta, G. Roff, M. Sigmond, and S. W. Son (2015), The predictability of the extratropical stratosphere on

https://doi.org/10.5194/acp-2021-646
Preprint. Discussion started: 25 August 2021

monthly time-scales and its impact on the skill of tropospheric forecasts, *Quarterly Journal of the Royal Meteorological Society*, 141, 987-1003, doi:10.1002/qj.2432.

Vigouroux, C., Blumenstock, T., Coffey, M., Errera, Q., García, O., Jones, N. B., et al. (2015). Trends of ozone total columns and vertical distribution from FTIR observations at eight NDACC stations around the globe. Atmospheric Chemistry and Physics, 15(6), 2915–2933. http://doi.org/10.5194/acp-15-2915-2015

Vigouroux, C., De Mazière, M., Demoulin, P., Servais, C., Hase, F., Blumenstock, T., et al. (2008). Evaluation of tropospheric and stratospheric ozone trends over Western Europe from ground-based FTIR network observations. Atmospheric Chemistry and Physics, 8(23), 6865–6886. http://doi.org/10.5194/acp-8-6865-2008

Wallace, J. M. (1973), General circulation of the tropical lower stratosphere, *Reviews of Geophysics*, *11*(2), 191–222, doi:10.1029/RG011i002p00191.

Wargan, K., C. Orbe, S. Pawson, J. R. Ziemke, L. D. Oman, M. A. Olsen, L. Coy, and K. Emma Knowland (2018), Recent Decline in Extratropical Lower Stratospheric Ozone Attributed to Circulation Changes, *Geophys. Res. Lett.*, *45*(10), 5166–5176, doi:10.1029/2018GL077406.

Wargan, K., G. Labow, S. Frith, S. Pawson, N. Livesey, and G. Partyka (2017), Evaluation of the Ozone Fields in NASA's MERRA-2 Reanalysis, *J. Climate*, *30*(8), 2961–2988, doi:10.1175/JCLI-D-16-0699.1.

Xie, F., Li, J., Tian, W., Fu, Q., Jin, F.-F., Hu, Y., et al. (2016). A connection from Arctic stratospheric ozone to El Niño-Southern oscillation. Environmental Research Letters, 11(12), 124026–12. http://doi.org/10.1088/1748-9326/11/12/124026

https://doi.org/10.5194/acp-2021-646
Preprint. Discussion started: 25 August 2021

Atmospheric Chemistry and Physics Discussions

Table 1. Site locations for NDACC FTIRs and ozonesondes. Uncertainties of FTIRs at three sites with ozonesondes are given by averaged subtraction and standard deviation of ozonesondes from the retrieved ozone from FTIR.

station	Longitude	Latitude	Solar FTIR Time period	Ozonesonde Availability period	%full PCO uncertainties	%Uncertainties 10 km -30km
Eureka	274	80	2006-now	1992-now	7% +/- 7%	1% +/- 7%
Ny-Ålesund	12	79	1995-now	1992-now	2% +/- 4%	7% +/- 8%
Thule	291	77	1999-now	1991-2016 (very sparse)	3% +/- 6%	3% +/- 6%
Summit Station	39	72	-	2005-2017		
Harestua	11	60	2009-now	-	-	
Kiruna	20	68	1997-now	-	-	

https://doi.org/10.5194/acp-2021-646
Preprint. Discussion started: 25 August 2021

Atmospheric Chemistry and Physics Discussions

Table 2. SSWs dates, duration, magnitude, and the duration of polar vortex from 2004 to 2020. The number of easterly days at 10 hPa over 60 N is shown as the duration SSW. The magnitude of SSWs is defined by the minimum zonal-mean zonal wind at 10hPa over 60 N during each SSW. The total number of easterly days associated with the event is not necessarily consecutive. The duration of polar vortex recovery is defined as the number of days that the zonal averaged EPV takes to reach the climatological zonal EPV.

SSWs date	Number of easterly days at 10 hPa over 60 N	Minimum zonal-mean zonal wind at 10hPa over 60°N (m/s)	Vortex recovery (days)
21 Jan 2006	26	-26	36
22 Feb 2008	15	-15	35
24 Jan 2009	30	-29	45
6 Jan 2013	22	-13	45
12 Feb 2018	19	-24	45
2 Jan 2019	21	-10	30

https://doi.org/10.5194/acp-2021-646
Preprint. Discussion started: 25 August 2021

Atmospheric Chemistry and Physics Discussions

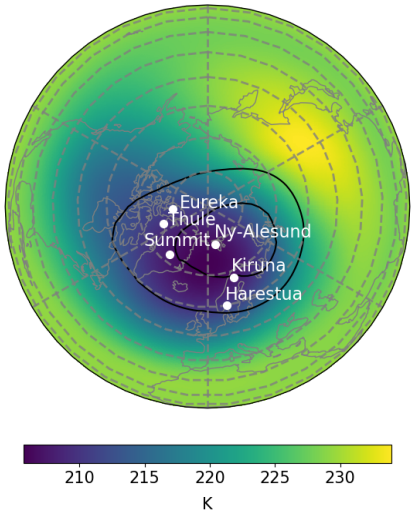

Figure 1. The climatology of temperature at 10 hPa and potential vorticity (PV) at the potential temperature of 850 K during wintertime (DJF) over the northern hemisphere. The climatology is based on non-SSW years from 2004 to 2019. The map coloring shows the average winter temperature. The black contour lines are 60 and 80 PV units (10^5 K m^2 Kg^{-1} s^{-1}). The locations of the observational sites are shown as white dots.

https://doi.org/10.5194/acp-2021-646
Preprint. Discussion started: 25 August 2021

Atmospheric Chemistry and Physics Discussions

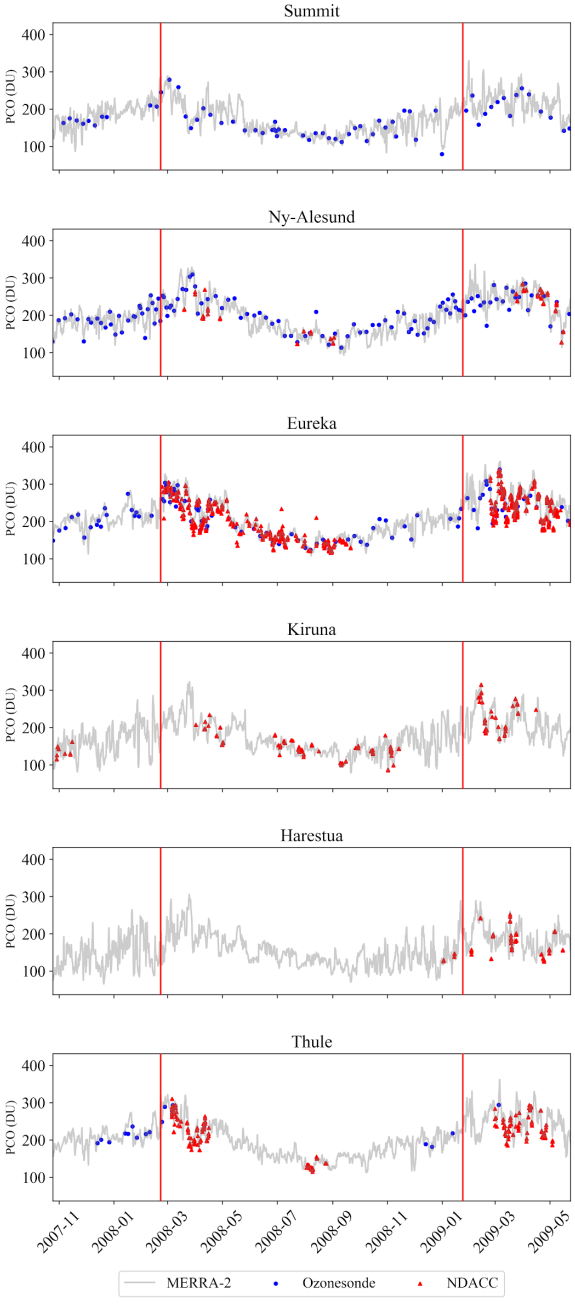

Figure 2. Time series of 3 hourly partial column ozone (PCO) of ground to 20 km derived from MERRA-2, solar FTIR, and ozonesondes at the study sites from winter 2007 to spring 2009. MERRA-2 is shown as the gray line. NDACC FTIR data and ozonesondes are shown as red triangles and blue circles, respectively.

https://doi.org/10.5194/acp-2021-646
Preprint. Discussion started: 25 August 2021

Atmospheric Chemistry and Physics Discussions

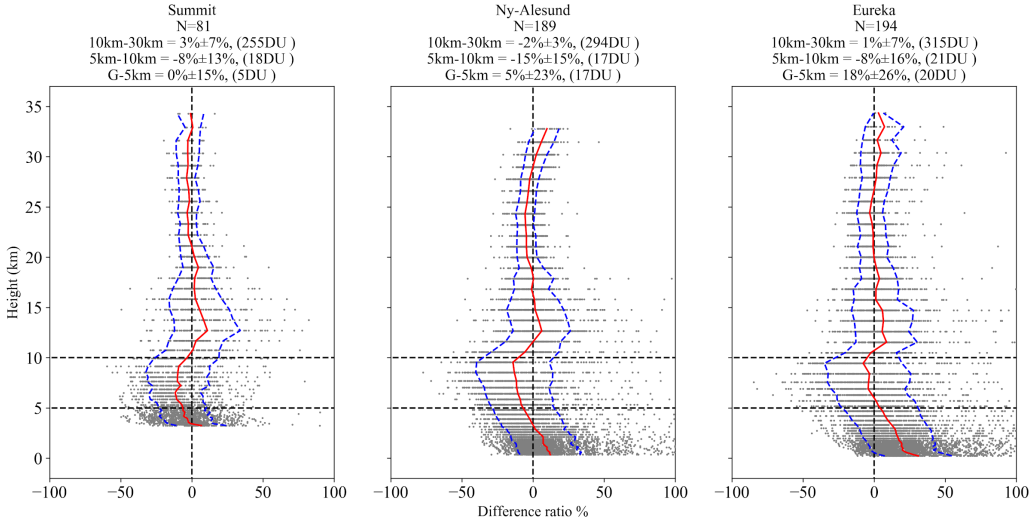

Figure 3. Difference ratios of ozonesonde and MERRA-2 at each layer at three sites from 1 Dec to 1 May for six year of SSWs. The difference ratio is the subtraction of ozonesonde from MERRA-2 ozone dataset divided by ozonesonde for each layer. The mean difference ratio is shown as the red line. The standard deviation of the difference ratio from the mean is shown at the blue line. The number of coincident ozonesonde and MERRA-2 comparisons between 1 Dec and 1 May for the six years of SSWs (N) is shown under each site name. The mean and standard deviation of PCO difference for 3 layers: 10km-30km, 5km-10km, Ground-5km are summarized for each site. The average PCO value for each layer is shown in parentheses.

https://doi.org/10.5194/acp-2021-646
Preprint. Discussion started: 25 August 2021

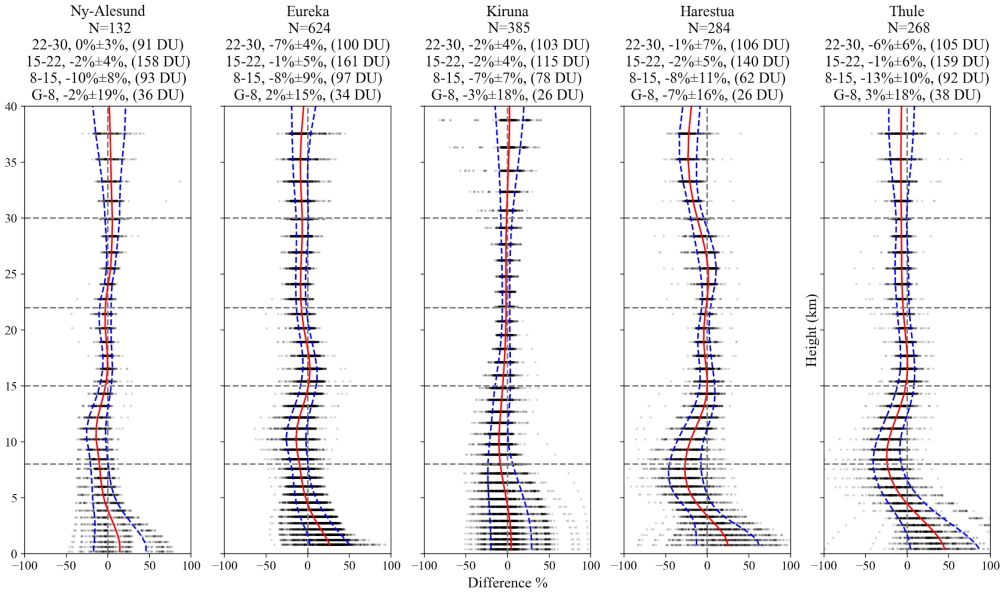

Figure 4. Difference ratios of FTIR retrieved ozone from MERRA-2. For each layer at each station, the mean ± standard deviation of NDACC retrieved ozone is subtracted from MERRA-2 and divided by retrieved value. The mean and standard deviation of difference ratios for each layer are shown as the red and blue lines. Statistical summaries of the MERRA-2 and NDACC comparisons in four layers of ground to 8 km, 8km-15km, 15km -22km, and 22km- 30km for each station are shown on top of each plot. Mean and standard ratio difference and the average PCO of each layer are shown for each site.

https://doi.org/10.5194/acp-2021-646
Preprint. Discussion started: 25 August 2021

Atmospheric Chemistry and Physics Discussions

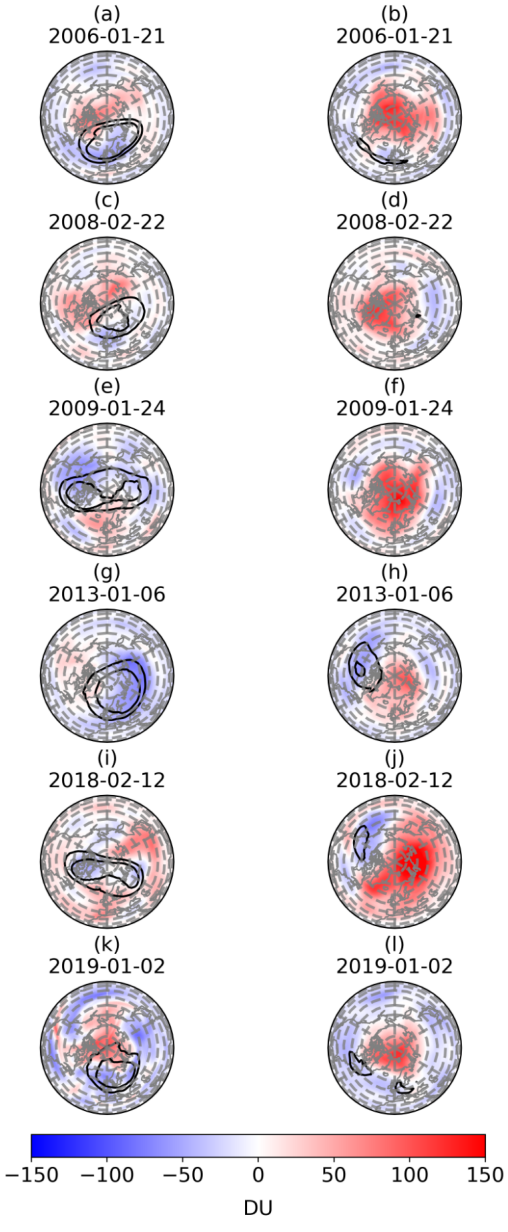

Figure 5. TCO anomaly using 15 days prior (first column) and 15 days after to each SSW (second column). PEV at the potential temperature of 850k is averaged for the same period similar to TCO. Contour lines show the EPV map at 60 and 80 10^5 K m^2 Kg^{-1} s^{-1}.

https://doi.org/10.5194/acp-2021-646
Preprint. Discussion started: 25 August 2021

Atmospheric Chemistry and Physics Discussions

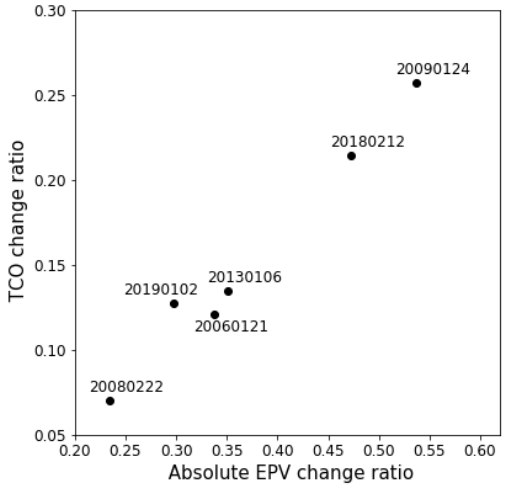

Figure 6. The zonally averaged EPV change ratio at the potential temperature of 850 K against the corresponding change in TCO for each SSW. The ratio of change for each variable is estimated as the average of 15 days after SSWs subtracted by the average of 15 days before the SSWs and divided by the average of 15 days before.

https://doi.org/10.5194/acp-2021-646
Preprint. Discussion started: 25 August 2021

Atmospheric Chemistry and Physics Discussions

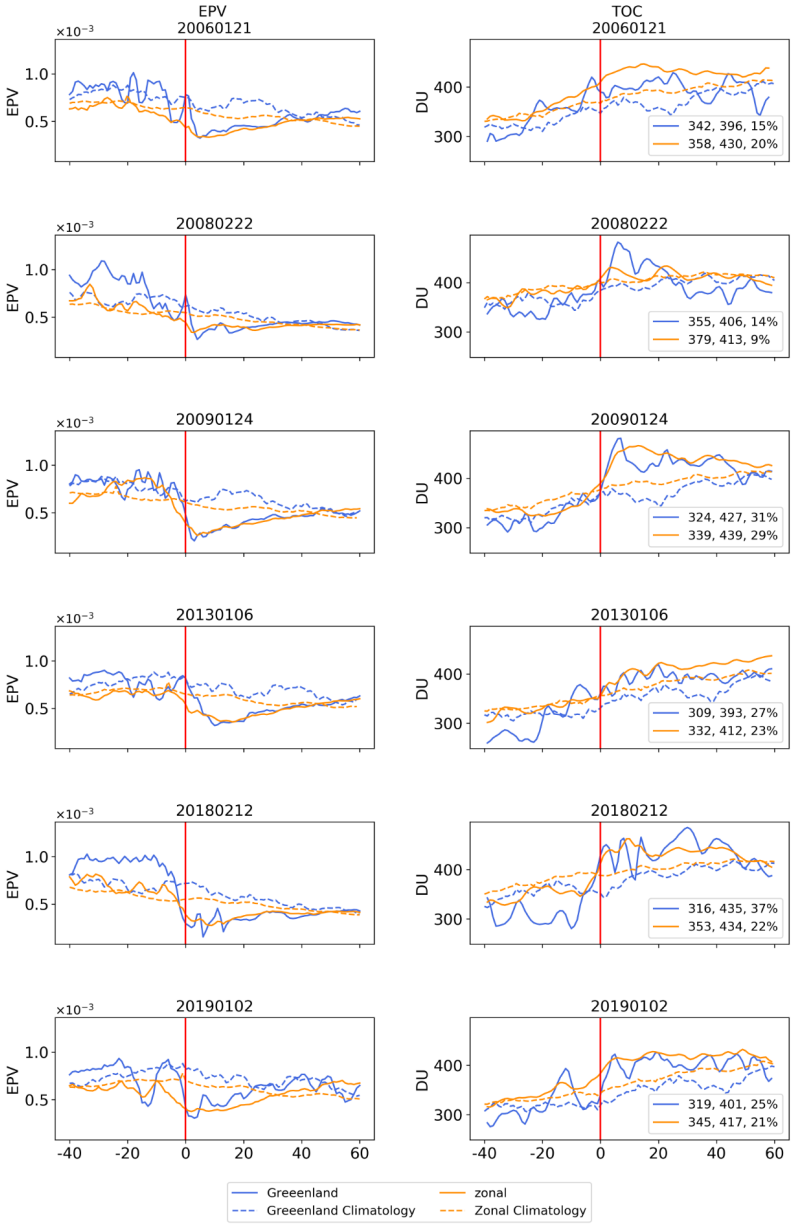

Figure 7. EPV at the potential temperature of 850k (first column) and TCO (second column) over the Arctic zonal mean 60-80N (orange line) and Greenland sector (blue line) during 40 days before and 60 days after each SSWs (each row). Climatology of EPV and TCO for the zonal and Greenland sector are shown in orange and blue dashed lines, respectively. The average Total Column ozone (TCO) during 40 days before and 60 days after, and the percentage of change for each SSWs are shown in the bottom corner of the second column.

https://doi.org/10.5194/acp-2021-646
Preprint. Discussion started: 25 August 2021

Atmospheric Chemistry and Physics Discussions

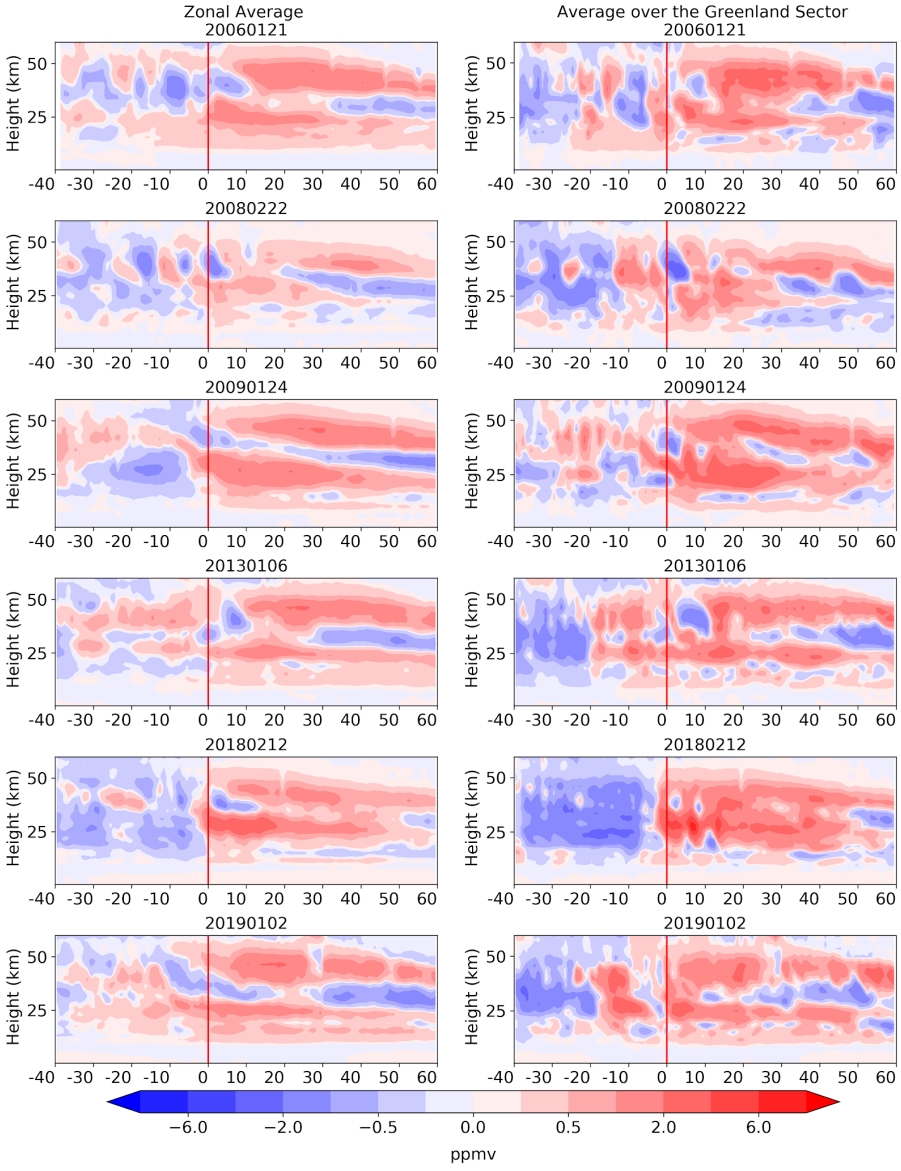

Figure 8. The cross section of ozone anomaly during 40 days before to 60 day of each SSWs averaged over the zonal averaged and Greenland sector. The vertical red line shows the SSWs incident date. Climatology was created using non-SSWs years since 2004. The vertical coordinate is the log-pressure height.

https://doi.org/10.5194/acp-2021-646
Preprint. Discussion started: 25 August 2021

Atmospheric Chemistry and Physics Discussions

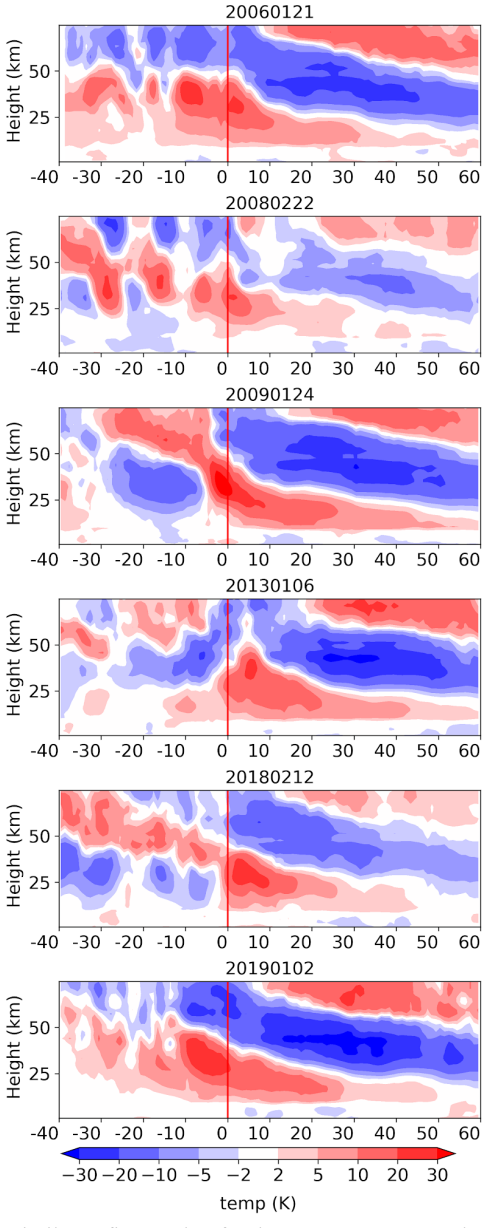

Figure 9. Similar to figure 8 but for the temperature anomaly for zonal average.

https://doi.org/10.5194/acp-2021-646
Preprint. Discussion started: 25 August 2021

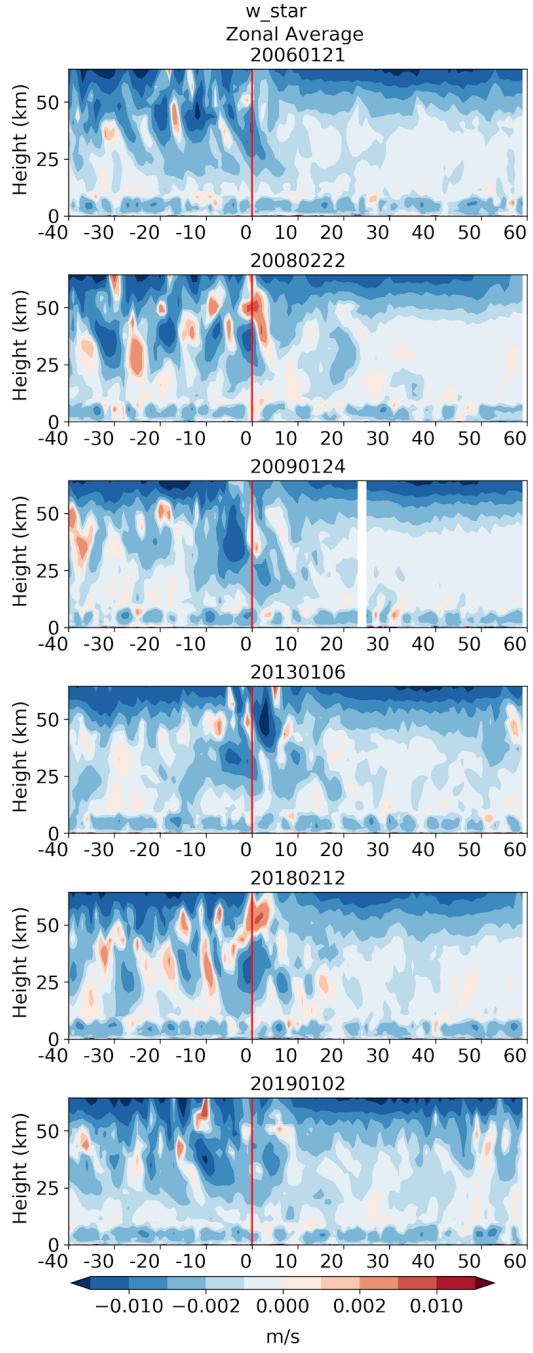

Figure 10. Similar to figure 8 but for the of the vertical component of the residual circulation, $\overline{w}^*$, for zonal average.

https://doi.org/10.5194/acp-2021-646
Preprint. Discussion started: 25 August 2021

Atmospheric Chemistry and Physics Discussions

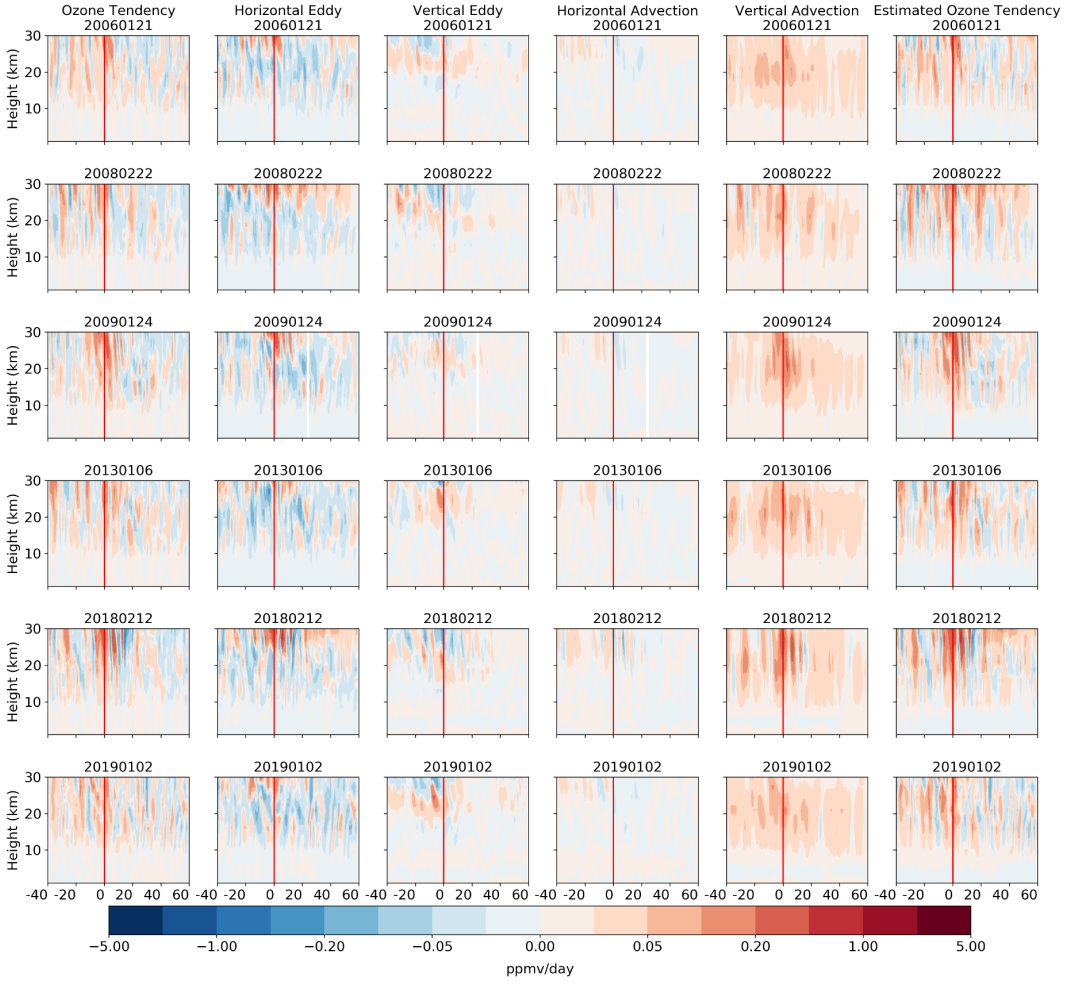

Figure 11. Same as Figure 8 for ozone tendency, horizontal and vertical component of eddy mixing, and horizontal $(-\overline{v}^* \overline{x}_y)$ and vertical $(-\overline{w}^* \overline{x}_z)$ component of mean advection, and the indirect ozone tendency using the right-hand side of equation (2). Summing four middle columns leads to the estimated ozone tendency on the sixth column. The vertical axis is the log-pressure height. The y axis is limited to 30 km to minimize the impact involved chemical processes on ozone evolution during SSWs.

https://doi.org/10.5194/acp-2021-646
Preprint. Discussion started: 25 August 2021

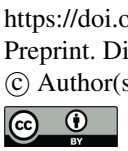

Atmospheric Chemistry and Physics Discussions

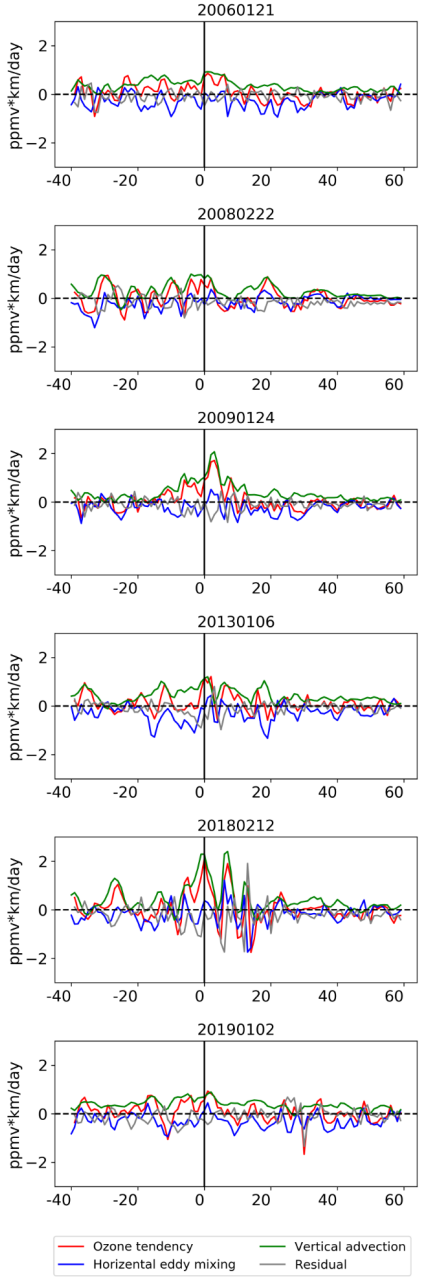

Figure 12. Time series of vertically integrated major elements of tracer continuity equation 2 from 15km to 30 km (Andrews et al, 1987). Ozone tendency is shown as the red line. The horizontal component of eddy mixing, $e^{(z/H)}dM_y/d_y$, is shown in blue line, the vertical component of vertical advection, $-\overline{w}^* \bar{x}_z$, is shown in the green line. The residual of all elements of tracer continuity is shown in the gray line.